

*University of Padova*

*Department of Information Engineering  
Department of Industrial Engineering  
Master Degree in Bioengineering*

MASTER THESIS

# **FE-Modelling and Material Characterization of Ice-Hockey Helmet**

*Student:*  
Isotta RIGONI

*Supervisor:*  
Prof. Nicola PETRONE  
*Co-supervisor:*  
Prof. Svein KLEIVEN

2nd of October 2017  
Academic year 2016/2017



## Abstract

The aim of this research was to produce a reliable finite element model of a helmet, that could be used to simulate approval tests as well as impacts to investigate the safety offered. A 2D and 3D mesh was generated from the CAD file of an Easton Synergy 380 with HyperWorks, and then checked referring to standard parameter values. A few specimens cut from the liner were tested with the Instron Electropuls E3000 (Instron, High Wycombe, Great Britain) machine to determine Young's modulus, Poisson's ratio and the density of the EPP. The numerical model was characterised with appropriate materials with Ls-PrePost, such as ABS for the shell, EPP for the liner and steel for the impact anvil. The foam was implemented both with the \*063\_CRUSHABLE\_FOAM and the \*126\_MODIFIED\_HONEYCOMB card, in two different configurations. The helmet model was coupled with a finite element model of a HIII head form and three impact scenarios were set up. Backward, lateral and pitched impact were simulated and results were compared with those obtained from the experimental tests carried on at the MIPS. The two configurations were tested in all the three scenarios. The correlation between numerical and experimental results was evaluated by analysing the linear and rotational acceleration, and the rotational velocity, recorded by the accelerometer positioned inside the HIII headform. The parameters used were the Pearson correlation coefficient, the peak linear acceleration score, the shape of the curves, the time occurrence of peaks and the percentage of the difference between them. The first configuration showed good correlation scores (>85%) for the backward and lateral impact, for the rotational velocity and acceleration, while lower values were recorded for the pitched impact simulation. Lower values (70.88% and 77.76%) were obtained for the peak linear acceleration score, which stress the need for modifications of the contact definition in Ls-PrePost or a more detailed material testing. Worse results were recorded for the second configuration, but the smaller computational time required suggests that more attempts should be done in this direction.



## **Acknowledgements**

I would like to thank my supervisor Prof. Svein Kleiven, who gave me the opportunity of working on such an interesting topic: thank you for your support and help, especially in the last weeks of the work. I stopped by your office definitely too many times in the last month, but you always welcomed me and came up with suggestions.

I would like to thank my Italian supervisor Prof. Nicola Petrone, who pushed me through my thesis once more, even though I wasn't the ideal student: we definitely obtained a more accurate and pleasing work.

I would like to thank Xiaogai Li, who offered me precious constructive critics and helped me structure and organise my thesis.

Another thanks must be addressed to Carl Magnusson and Gustav Söderström, who helped me in the realization of this project providing me the material properties of the foam. It was a pleasure to test EPP with you.

A big thanks goes to all the PhD students who were with me in these months: it was a pleasure to be in your office and thank you for making my 2-days-to-thesis-submission-birthday special. In particular, I would like to thank Madelen Fahlstedt for all the questions she answered, even though she did not have to. And last but not least, Annaclaudia, who before being a helpful biomechanical researcher, was a friend. Thank you for all the chatters and for the several suggestions you gave me: it would have been much more difficult without you!

Another special thanks goes to Silvia, Giuliana and Hildi, whose name I am still not able to pronounce. You were the best desirable supervision group: thank you for the feedbacks and the good time we spent together.

A huge overseas english thanks goes to Giulio, who helped me more than anyone else. Thank you for listening to all my doubts and problems, and for always suggesting, even on the choice easiest to take. Thank you for accepting me the way I am, without asking me to change but just to work on myself. You are the best person I could have ever asked for: thank you for loving me freely. And most important: thank you for having made 2000 km distance our biggest strength.

At the end, a special overseas thanks must go to my family and my friends back home: even though we are thousands of kilometers apart, I have never felt you closer than I do now.



# Table of Contents

|   |           |
|---|-----------|
| <b>1 Introduction</b>                                       | <b>3</b>  |
| <b>2 Methods</b>  | <b>5</b>  |
| 2.1 GEOMETRY CLEANING AND MESHING OF THE HELMET             | 5         |
| 2.1.1 <i>Shell</i>  | 5         |
| 2.1.2 <i>Liner</i>  | 7         |
| 2.2 MATERIAL TESTING  | 7         |
| 2.3 SIMULATION SET UP – FIRST MATERIAL MODEL CONFIGURATION  | 10        |
| 2.3.1 <i>Helmet model – Material Characterization</i>       | 10        |
| 2.3.2 <i>Positioning of the Hill head model</i>             | 10        |
| 2.3.3 <i>Experimental Drop Tests</i>                        | 11        |
| 2.3.4 <i>Drop Test Simulations</i>                          | 13        |
| 2.4 SIMULATION SET UP – SECOND MATERIAL MODEL CONFIGURATION | 14        |
| 2.5 CORRELATION METHODS                                     | 14        |
| 2.5.1 <i>Correlation Coefficient</i>                        | 14        |
| 2.5.2 <i>Peak Linear Acceleration Score</i>                 | 15        |
| <b>3 Results</b>  | <b>17</b> |
| 3.1 MESH AND QUALITY CHECK                                  | 17        |
| 3.2 FOAM PROPERTIES   | 19        |
| 3.3 SIMULATION RESULTS                                      | 21        |
| 3.3.1 <i>Results- First Configuration</i>                   | 21        |
| 3.3.1.1 <i>Correlation Coefficient</i>                      | 22        |
| 3.3.1.2 <i>Peak Linear Acceleration Score</i>               | 24        |
| 3.3.2 <i>Results-Second Configuration</i>                   | 24        |
| 3.3.2.1 <i>Correlation Coefficient</i>                      | 25        |
| 3.3.2.2 <i>Peak Linear Acceleration Score</i>               | 27        |
| <b>4 Discussion</b>   | <b>29</b> |
| <b>5 Conclusion</b>   | <b>33</b> |
| <b>APPENDIX A</b>   | <b>35</b> |



# 1 Introduction

Traumatic brain injuries (TBIs) are estimated to be one of the most common and dangerous sport-related accidents: among every two million new TBI cases that occur annually in the United States, 300 000 are linked to sports [1]. In ice-hockey, TBIs account for 10-15% of all injuries [2]: only in 2009, 8154 cases of TBIs were recorded in America among ice-hockey players [3].

Concussions are believed to be the most frequent TBI occurring in ice-hockey and in sports in general [4]: 20% of all professional hockey players are likely to experience at least one concussion, during their whole career [5]. Concussions are defined as a mental status alteration, induced by a trauma, that may be characterized by confusion, amnesia and possible loss of consciousness [1].

To prevent sport-related head injuries, protection systems need to be improved and optimised. Three main methodologies are available nowadays to study the biomechanics of injuries: Anthropometric Test Device (ATD) simulations, Post Mortem Human Subject (PMHS) simulations and mathematical model simulations [6], of which, finite element (FE) models are the most spread (see Appendix). In contrast to ATDs and PMHSs, the use of FE models allows repeatable and reproducible simulations [7], with the possibility of measuring quantities such as Von Mises (VM) stress, longitudinal strain [8], rotational and linear acceleration [9] and impact duration [10].

FE models of helmets have been used to investigate different aspects of impacts, such as the role of rotational acceleration, which has turned out to be more dangerous than the linear one [8], and to study properties of materials composing the helmet itself, in order to compare different material combinations for deciding on the most protective one [9].

While FE models have been developed for bicycle [11], equestrian [8], motorcycle [9] and other helmets, to the best knowledge of the author no finite element model is available for ice-hockey helmet, which means that no simulations can be performed to reproduce a possible game impact.

The aim of this thesis is to develop a FE model of an ice-hockey helmet that has not been brought to the market yet and to characterize its material properties. Material tests on the foam will be performed in order to approximate its properties to their actual values, so that they can be implemented into the FE model.

The final step is then to validate the latter by reproducing a drop test, previously performed at the laboratory of the Multi-directional Impact Protection System (MIPS), and comparing the results of the simulations with those of the real test in terms of six degrees of freedom (DOF) acceleration.

## 2 Methods

### 2.1 Geometry Cleaning and Meshing of the Helmet

The helmet modelled in this thesis is the Easton Synergy 380, which was previously tested at the MIPS, the company that provided the Computer-Aided Design (CAD) files with the original geometry.

The FE model was developed from the CAD file used to mould the helmet, shown in Fig.1. The original geometry was modified to make the meshing procedure easier, by dividing the whole helmet into two halves. Both the geometry cleaning and the 2D-3D meshing were performed on one half and then mirrored to the other, selecting the y-axis as the one perpendicular to the plane of reflection. Both the shell and the foam were meshed with the software Altair|HyperWorks® 2017 Student Edition [12].

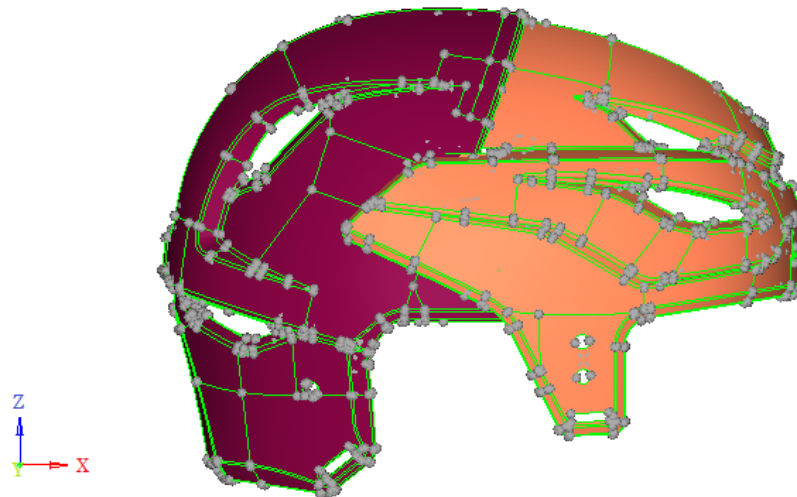


**Fig. 1:** Original CAD geometry of the shell; green lines are shared edges and grey points are fixed points. The front and the back shell are shown in pink and violet, respectively.

#### 2.1.1 Shell

The geometry of the shell was simplified as much as possible to create surfaces that were easier to mesh. Since the size of the element was set to 5 mm and the distance between the inner and the outer shell was less than 3 mm, the inner one was deleted. The original shell thickness will be restored before running simulations. To

create continuity in the mesh, the front and the back shell (see Fig.1) were melted together in a single surface. All the holes with diameter less than 7 mm were closed and most of the lines were suppressed, not to make the mesh follow undesired directions, as it can be seen in Fig.2.

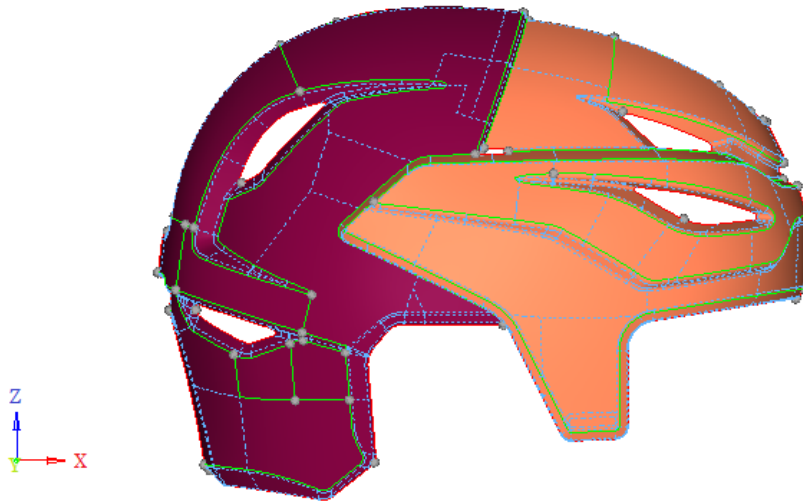


**Fig. 2:** Simplified shell surfaces, obtained by the suppression of undesired lines, the filling of small holes and the removal of some points; red lines are free edges and blue lines are suppressed edges.

As mentioned before, the 2D element size was set to 5 mm to reduce the computational time for simulations. The 2D mesh was obtained with the “automesh” option and both triangular and quadrilateral elements were accepted, by using the “mixed” mesh type. To have a uniform and clear mesh, the number of elements per side were adjusted using the “density” function and some lines were suppressed. The obtained 2D mesh is shown in Fig.3.

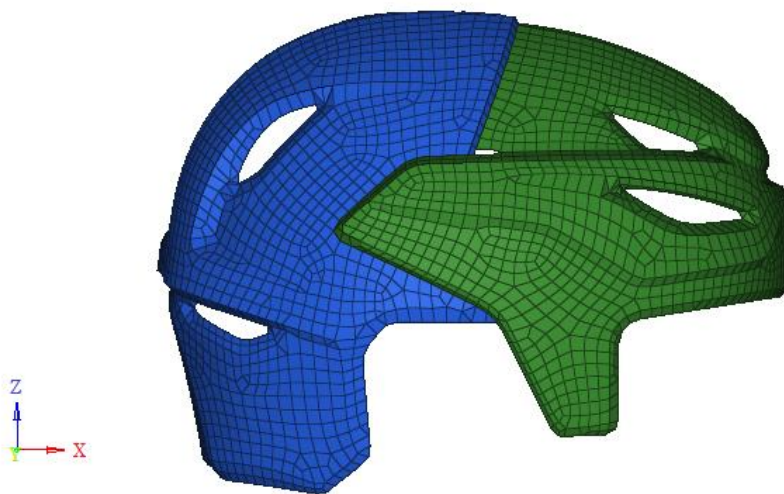


**Fig. 3:** Generated FE mesh of the helmet shell.

The quality of the mesh was checked by evaluating the following predefined parameter values:

- the warpage value of quads elements, which describes how much an element deviates from being planar: a quad element is split into two trias by dragging one of its diagonals and the angle between the normals to the two halves is calculated;
- the aspect ratio value, which is usually calculated as the ratio between the longest element edge and its shortest edge;
- the skew value, which is obtained -for trias elements- by calculating the minimum angle between the median of each edge and the vector connecting the two adjacent mid-sides, and subtracting it from 90°; for quads, the angle calculated is the minimum between the two lines connecting opposite mid-sides of the element;
- the minimum/maximum allowable interior angle;
- the jacobian value, which describes the element deviation from its ideal shape, which corresponds to a value of 1 [13].

### **2.1.2 Liner**

The liner was divided into three sub-components, i.e. front, lateral and back liner. Moreover, to make each solid mappable, the liner components were split into smaller volumes and most of the lines were suppressed. A solid is defined mappable if it shows the following characteristics: i) it encloses a closed volume; ii) it has one or multiple source surfaces but only one destination surface; iii) there are no edges perpendicular to the drag direction [14].

Because the geometry of the liner is very irregular, not all the sub-volumes were made mappable. The automatic HyperWorks' meshing command could not be used for those still unmappable. An alternative solution was used to solve the problem, i.e. first the surface of the single solid was meshed, then the 2D element quality was checked, to make sure that the two dimensional mesh was the best possible and then the mesh was extruded along the drag surface to create a 3D mesh. In this way, since both quadrilateral and triangular elements were accepted for the 2D mesh, the solid elements created were both hexahedron and pentahedron.

After the solid mesh was created, its quality was checked referring to the same parameters considered for the 2D mesh.

## **2.2 Material Testing**

To implement correct material properties into the model, the foam of the liner was tested in a laboratory. The liner was made of Expanded Polypropylene (EPP), but more specific material properties were required for setting the simulations in the

software, i.e. the stress-strain curve, the Young's modulus and the density. The plastic shell of the helmet was not tested, since it was recognised to be Acrylonitrile butadiene styrene (ABS), and its mechanical properties are known from literature.

Two test designs were applied to two set of samples, composed by five and four samples each. The samples were obtained from five parts of the helmet (as shown in Fig.4): their shape was cylindrical, with the ratio between height (H) and diameter (D) having an average value of 1.3414. The ideal value of the H/D ratio is between 1.5 and 2, where the upper limit represents the maximum allowable value to avoid the buckling of the foam [15]. Regarding the samples analysed, their H/D ratios were the best achievable with the available instrumentation. Since they were obtained directly from the foam of the liner, which did not show a constant thickness, their diameter was constantly 6 mm, while their height was variable.

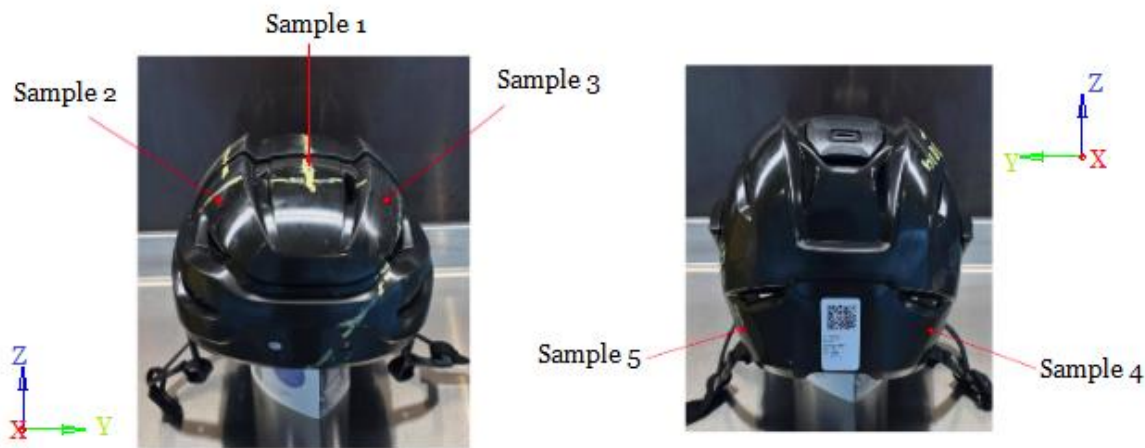


**Fig. 4:** Front (left) and back (right) view of the helmet: the five zones are those from where the samples were obtained.

In the first test session, four samples –obtained from zone 2 and 3, which were the thickest ones- underwent a compression at four different strain rates, to investigate the dependency of the foam characteristics on the applied strain rate. Strain rates of 0.01, 0.1, 1 and 10 were applied with the 5 kN load cell of the Instron Electropuls E3000 (Instron, High Wycombe, Great Britain) and the correspondent stress-strain curves were registered.

In the second test session, five samples from the five zones (see Fig.4) were tested with the Instron Electropuls E3000 (Instron, High Wycombe, Great Britain) at a constant strain rate of 10/s, which means that the compression displacement of 9 mm was performed at a speed of 90 mm/s. This experiment was chosen to check whether there were differences in the material response of the five different parts of the helmet.

The other properties were evaluated with different methodologies, to give a better description of the behaviour of the foam.

The Young's modulus describes the stiffness of the solid material: it is defined as the ratio between the applied stress and the derived strain. It can also be defined as the gradient of the linear elastic region (see Appendix), which is the first part of the stress strain curve [16], as shown in Fig.5. Five different Young's moduli were calculated from the curves recorded in the first test by evaluating the gradient between the origin of the curve and where the plateau starts, and results were then averaged.

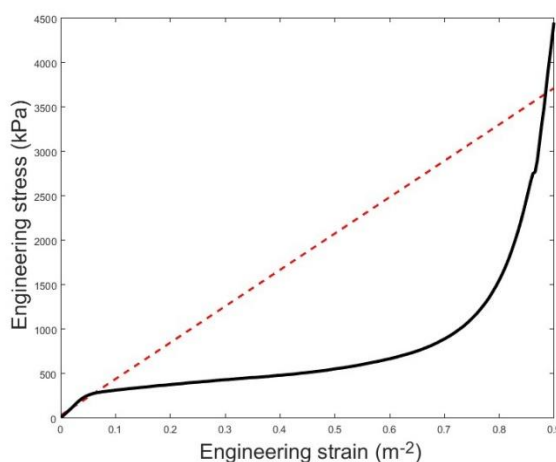


**Fig. 5:** Stress strain curve (black) of an EPP specimen and the line (red) that better approximate the linear elastic region curve, obtained with linear regression, used to evaluate the Young's moduli.

The density was measured by calculating the ratio between the mass of one sample and its volume. The mass was obtained with the help of a high sensitivity scale, while the volume was calculated with

$$V = r^2 * h * \pi \quad (1)$$

where  $r$  is the radius and  $h$  is the height of the sample.

The two experiments were recorded with the Sony CyberShot DSC-RX10 II high speed camera, in order to estimate the Poisson's ratio value from the transverse deformation undergone by the foam during the longitudinal compression [17]. The transverse strain was evaluated through video analysis of the recorded experiments.

## 2.3 Simulation set up – First Material Model Configuration

The FE model of the helmet was manipulated with LS-PrePost® V4.3 [18], a pre- and post- processor by LSTC, in order to characterise its material properties. Two different material configurations were generated starting from the same FE model of the helmet: they mainly differ in the material cards used and in the definition of the contacts (see section 2.4 for the second configuration). The FE helmet model was then coupled with the FE Hybrid III (HIII) model to simulate three impact tests performed at MIPS. The simulations were run using the software LS-DYNA (version R8.0.0, revision 95309) [19].

### 2.3.1 Helmet model – Material Characterization

The shell of the helmet was implemented with material \*001\_ELASTIC, which characteristics were taken from the literature [20]. As mentioned in section 2.1.1, the shell was assigned a thickness of 0.003 m, by selecting the default element formulation “Belytschko-Tsay”. Values can be seen in Table 1.

The helmet liner was modelled with material \*063\_CRUSHABLE\_FOAM and the foam properties implemented are those that resulted from the laboratory experiments (see Results 3.2). The element formulation selected was the option “fully integrated S/R solid”.

**Table 1:** ABS and EPP properties implemented in the FE model.

| Material  | Density (Kg/ m <sup>3</sup> ) | Young’s Modulus (Pa) | Poisson’s Ratio | Damping Coefficient |
|-----------|-------------------------------|----------------------|-----------------|---------------------|
| ABS shell | 1390.0000                     | 1.867e+009           | 0.3500000       | -                   |
| EPP liner | 54.400002                     | 5.240e+006           | 0.0050000       | 0.0600000           |

The contact used between the shell and the liner was the \*CONTACT\_TIED\_SURFACE\_TO\_SURFACE\_OFFSET: the definition of an offset was necessary because of the presence of some voids between the shell and the foam. The shell was assigned the master part with a scale factor for master surface thickness (SFMT) of 10.0, while the liner was assigned the slave part with scale factor on default slave penalty stiffness (SFS) of 10.0. An additional \*CONTACT\_AUTOMATIC\_SURFACE\_TO\_SURFACE card was set between the two parts to avoid penetrations.

### 2.3.2 Positioning of the HIII head model

The FE model of the HIII headform was manually positioned inside the FE model of the helmet. The size of the helmet was scaled along the longitudinal direction of 3% of the total length, and of 2% of the total width along the transverse direction.

The initial penetrations were then checked with the option “Contact Check” and the nodes of the foam which were penetrating the dummy head surface were relocated with the automatic option “fix”.

The contact between the two models was defined with the \*CONTACT\_AUTOMATIC\_SURFACE\_TO\_SURFACE card. After some parametric studies were performed, the friction coefficient was set to 0.5. The dummy head model was set as the master segment with a scale factor on default master penalty stiffness (SFM) of 0.25 because of the high difference in the stiffness between the materials of the two parts entering in contact. Moreover, in order to avoid penetrations, a shell was created on the surface of the foam, which was defined with the \*009\_NULL card and a thickness of 0.002 m.

### 2.3.3 Experimental Drop Tests

Simulations were performed at the MIPS in order to evaluate the level of safety offered by the helmet. Three oblique impacts were tested with the oblique test rig shown in Fig.6: a Hybrid III head form was secured to an Easton Synergy 380 helmet, and they were made impact a 45° angled steel anvil from a drop height of 2.2 m [21]. The friction coefficient between the helmet shell and the anvil was measured to be 0.7.



**Fig. 6:** The oblique test rig used to perform the three drop tests at the MIPS. The 45° angled steel anvil is shown on the right.

The Hybrid III dummy head was equipped with a nine accelerometers system mounted according to the 3-2-2-2 method described in [22]: three accelerometers positioned at the centre of gravity (COG) of the head form and two extra

accelerometers mounted at the end of each axis, as shown in Fig.7. A view of the placement of the accelerometers inside the Hybrid III head form is offered in Fig.8.

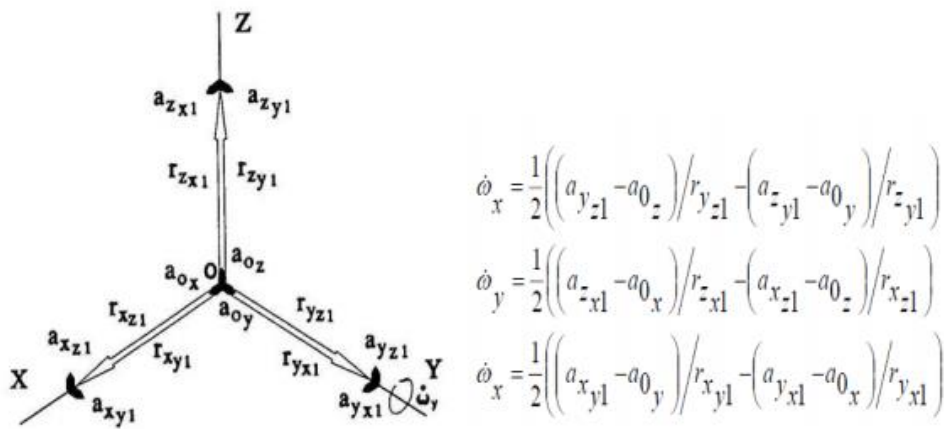


Fig. 7: Schematic view of the accelerometers functioning and rotational acceleration equations [23].

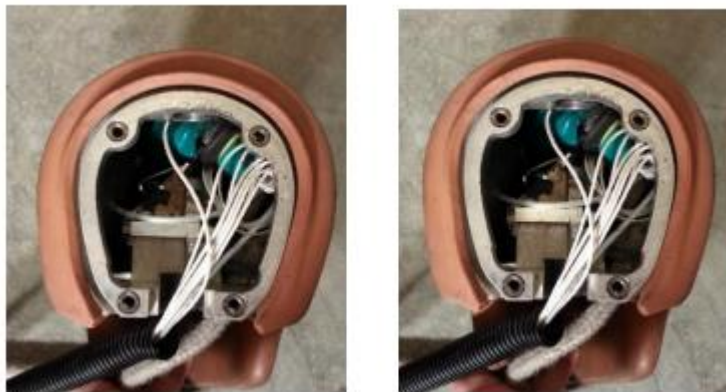
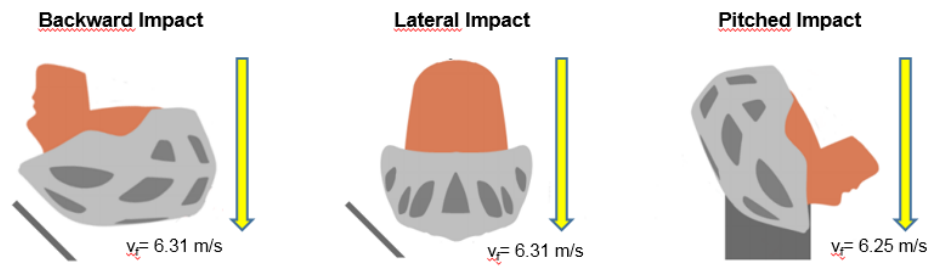


Fig. 8: View of the positioning of the accelerometers inside the dummy head.

The accelerometers were manufactured by Dytran Instruments, Inc. and their range was of 500 g. Four of them were the 3032A model, while the rest were model 3015. The translational acceleration was measured with the three accelerometers positioned at the COG of the head form, while the rotational acceleration and velocity were recorded by the whole system of accelerometers: they were collected through the LabView software, which used a computer code developed at the KTH, Stockholm [24].

Three impacts were investigated, which are those shown in Fig. 9:

- 1) Backward impact; the velocity reached at the impact time was 6.31 m/s in the vertical direction;
- 2) Lateral impact; the final velocity was 6.31 m/s in the vertical direction;
- 3) Pitched impact; the final velocity was 6.25 m/s in the vertical direction.



**Fig. 9:** Three impact test designs, shown for a bicycle helmet (Modified by [21]).

### 2.3.4 Drop Test Simulations

Three simulations were set up with LS-PrePost® V4.3, which reproduced the three impact conditions. The 45° angled steel anvil was modelled with the \*O20\_RIGID material, which was characterised with the mechanical properties shown in Table 2 [25]. The contact between the shell of the helmet and the anvil was defined as a \*CONTACT\_AUTOMATIC\_SURFACE\_TO\_SURFACE, with a coefficient of friction of 0.7, as suggested from the collaborators from the MIPS and further confirmed by parametric studies performed on LS-DYNA. The FE model of the anvil was constrained in order not to be subjected to any displacement.

**Table 2:** Steel material properties [25], used to implement the anvil in the simulations

| Material | Density (Kg/ m <sup>3</sup> ) | Young's Modulus (Pa) | Poisson's Ratio |
|----------|-------------------------------|----------------------|-----------------|
| Steel    | 7800.00                       | 2.00e+011            | 0.25            |

The termination time was set to 0.02 s, in accordance to the duration of the recorded experiment. The time step was set to 0.6. The FE model of the helmet (coupled with the HIII head form) was positioned as close as possible to the anvil surface and it was given the correspondent initial velocity with the \*VELOCITY\_GENERATION card, in order to simulate the drop height of 2.2 m. For each test design, the dummy-and-helmet model was rotate and translate to reach the best configuration, as shown in Fig.10.

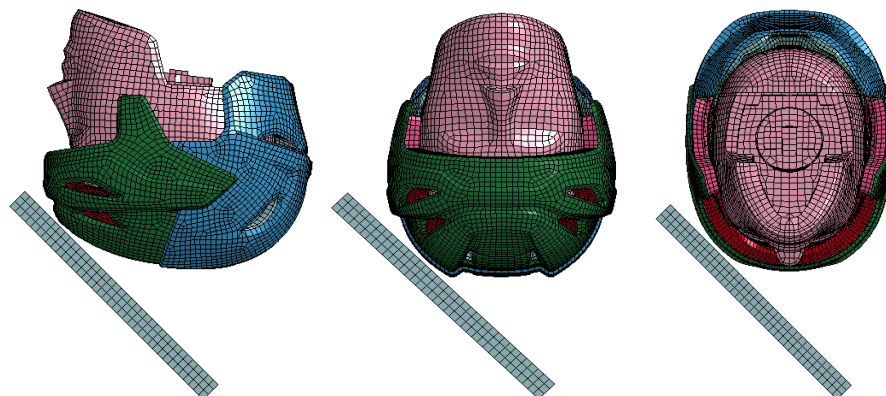


**Fig. 10:** Simulation set up for the backward impact (left), for the lateral impact (middle) and for the pitched impact (right).

The linear acceleration, the rotational velocity and the rotational acceleration were recorded at the central node of the FE model of the accelerometer, positioned at the centre of mass (COM) of the HIII head form model, as shown in Fig.11.

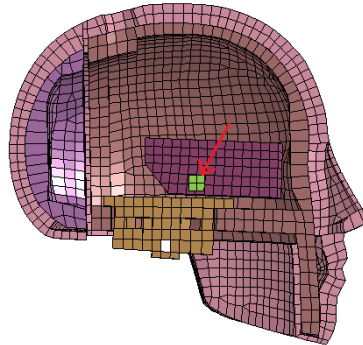


**Fig. 11:** Cross sectional view of the FE model of the HIII head form: the accelerometer positioned at the COM of the model is the one indicated by the arrow.

## 2.4 Simulation set up – Second Material Model Configuration

A second configuration was generated from the one described in section 2.3, which implied the change of the material used to model the foam and some other minor modifications. The liner was modelled with the \*126\_MODI-FIED\_HONEYCOMB card, implemented with the EPP properties obtained in the laboratory. Because the shear strain curve was required and it was not available, a previously measured shear strain curve of Expanded Polystyrene (EPS) was used. The shell meshed on the foam surface was characterised with a \*001\_ELASTIC material, with the same density, Young's modulus and Poisson's ratio of the liner. The contact between the shell and the liner was established between the ABS liner and the elastic internal shell with a \*CONTACT\_TIED\_SHELL\_EDGE\_TO\_SURFACE\_BEAM\_OFFSET contact card, where both the master and the slave part were assigned a scale factor for slave surface thickness (SFST) and SFMT of 10.0. An additional \*CONTACT\_AUTOMATIC\_SINGLE\_SURFACE contact was defined for the shell meshed on the foam in order to prevent bottoming out. The coefficient of friction was set to 0.3 between the liner shell and the head form model and SFST was set to 0.1.

## 2.5 Correlation Methods

### 2.5.1 Correlation Coefficient

The linear acceleration, the rotational velocity and the rotational acceleration curves obtained from the simulations were filtered with the SAE 300 low pass digital filter in LS-DYNA and were then manipulated with MATLAB® R2016b [26]. The Pearson coefficient  $r$  was evaluated to describe the strength of the linear relationship between the curves registered during the simulations and those

provided by the MIPS [27]. The value of  $r$  ranges from -1 to +1, to indicate a strong negative or positive linear relationship, respectively [28]:

$$r = \frac{\sum_{i=1}^n (x_i - \bar{x})(y_i - \bar{y})}{\sqrt{\sum_{i=1}^n (x_i - \bar{x})^2 \sum_{i=1}^n (y_i - \bar{y})^2}} \quad (2)$$

where the two variables are  $x$  and  $y$ , and the others the mean values. If the value of  $r$  is close to 1, the points lie on a straight line on the scatter diagram, to indicate that one variable increases with the other, as shown in Fig.9. On the other hand, if  $r$  is close to 0, it can indicate either the absence of a linear relationship or the presence of a nonlinear one between the two variables (Fig.12).

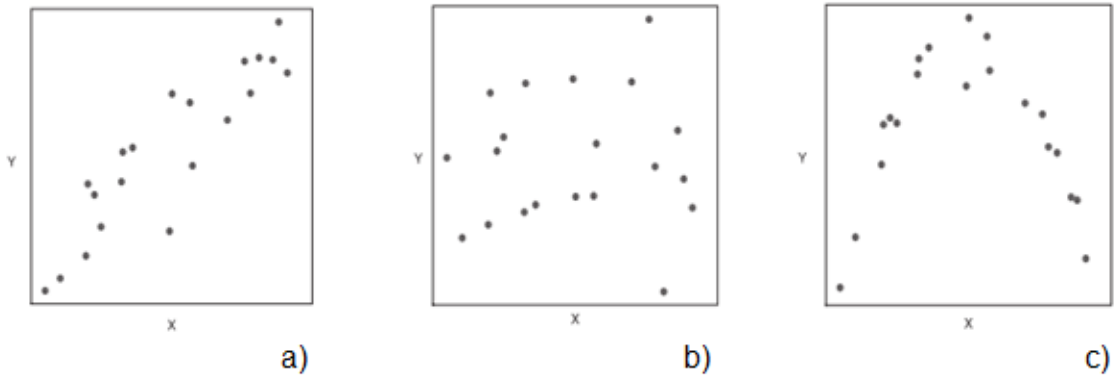


**Fig. 12:** Scatter diagram for variables X and Y; a)  $r=0.9$ , positive linear relationship; b)  $r=0.04$ , no linear relationship; c)  $r=-0.03$ , nonlinear relationship [28].

The shape of the curves and the occurrence of peaks were evaluated in order to establish the correlation between the two data sets as well as the percentage of the difference between the peaks. This last one was calculated with the formula:

$$[\%] = \frac{100 * |TV - SV|}{TV} \quad (3)$$

where TV is the test value and SV the simulation value.

### 2.5.2 Peak Linear Acceleration Score

The peak linear acceleration score was used to calculate the correlation between the peak values measured from the simulations and those of the drop tests. The formula used is the following, where PS is the peak score, TV is the test value and SV the simulation value [27]:

$$PS = \left[ 1 - \frac{|TV - SV|}{|TV|} \right] * 100\% \quad (4)$$

A value of 0% is considered as an indicator of a bad correlation between the linear acceleration peak measured from the model and the one recorded during experiments; a value of 100% indicates a perfect correlation between the two peaks. Values more than 80% describe a good correlation between the peaks [27].

## 3 Results

### 3.1 Mesh and Quality Check

The final model is made of 5412 shell elements (quadrilateral and triangular) and 18486 solid elements (hexaedron and pentahedron). The model is divided into five parts, which are back and front shell and front, lateral (two) and back foam, as shown in Fig.13.

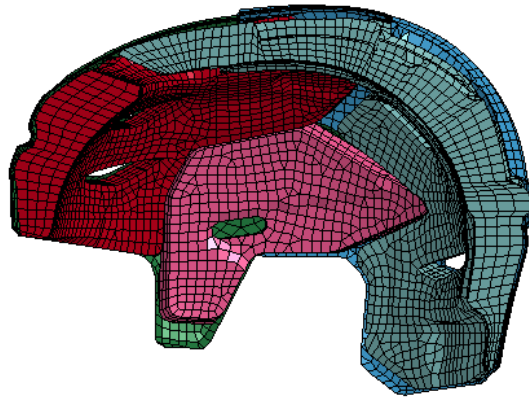


**Fig. 13:** A cross section view of the FE model of the foam (red, pink and grey) and the shell (green and blue).

The quality of the mesh was checked using the same criteria as used in the GHBMC project [29] through the function “check elems” of Hyperworks (Fig.14).

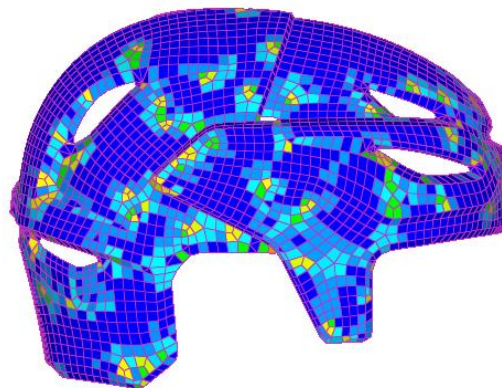


**Fig. 14:** Quality Check performed on the shell for the Jacobian parameter, where red elements represent those which do not meet the target.

Those shell and solid elements that did not meet the set target were modified either manually or with automatic options offered by HyperWorks. The final results are reported in Table 3, where the percentage of elements not meeting the target is indicated and the minimum or maximum value reported for each parameter is shown.

**Table 3:** Quality check table used to assess the mesh quality of the model.

|              |                                  | <b>Element Measure</b> | <b>Target Soft Limit (99%)</b> | <b>Failed Elements</b> | <b>Min/Max value</b> |
|--------------|----------------------------------|------------------------|--------------------------------|------------------------|----------------------|
| <b>SHELL</b> | <b>QUAD</b>                      | Warpage                | < 30°                          | 0%                     | 76.45                |
|              |                                  | Aspect ratio           | <6°                            | 0%                     | 8.23                 |
|              |                                  | Skew                   | <60°                           | 0%                     | 59.79                |
|              |                                  | Jacobian               | >0.5                           | 0%                     | 0.43                 |
|              |                                  | Min angle              | >30°                           | 0%                     | 40                   |
|              |                                  | Max angle              | >150°                          | 0%                     | 139.98               |
|              | <b>TRIA</b>                      | Aspect ratio           | <6°                            | 0%                     | 8.23                 |
|              |                                  | Skew                   | <70°                           | 0%                     | 59.79                |
|              |                                  | Min angle              | >30°                           | 6%                     | 18.74                |
|              |                                  | Max angle              | <150°                          | 0%                     | 117.34               |
| <b>SOLID</b> | <b>HEXAEDRON AND PENTAHEDRON</b> | Warpage                | <50°                           | 1%                     | 179.99               |
|              |                                  | Aspect ratio           | <8°                            | 0%                     | 23.58                |
|              |                                  | Skew                   | <70°                           | 1%                     | 89.22                |
|              |                                  | Jacobian               | >0.4                           | 1%                     | -10.80               |
|              |                                  | Quad face min angle    | >30°                           | 2%                     | 0.80                 |
|              |                                  | Quad face max angle    | <150°                          | 3%                     | 358.96               |
|              |                                  | Tri face min angle     | >15°                           | 1%                     | 6.10                 |
|              |                                  | Tri face max angle     | <140°                          | 1%                     | 155.47               |

Although the target percentages were met, the minimum value of the Jacobian of solid elements was negative, which prevented simulations to start. The final solid mesh was then re-checked with Ls-PrePost, checking the value of the Distortion Index (DI) and the element volume (Fig.15). The elements (85) which DI was less than 0.1 or had a negative volume were manually modified, by repositioning their nodes. Because of the rung shaped top of the back foam, elements were extremely distorted: 40 of them were simply deleted, since their shape prevented nodes to be picked up and then moved to a new location.

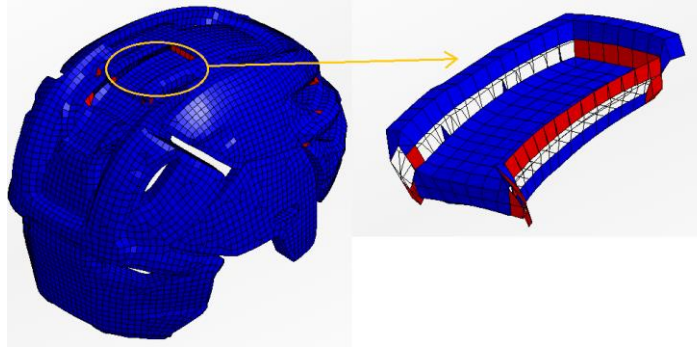


**Fig. 15:** Quality check for solid elements with  $DI < 0.1$ : red elements are those which do not meet the target (left); ring-shaped top of the back foam, which elements were deleted (right).

### 3.2 Foam Properties

The stress strain curves recorded during the two sessions of experiments were analysed and elaborated: instead of measuring both the loading curve, due to the compression of the specimen, and the unloading one, only the first one was registered and then plotted. In Fig. 16, the four curves describe the behaviour of the EPP when exposed to different strain rates. An average curve was also calculated.

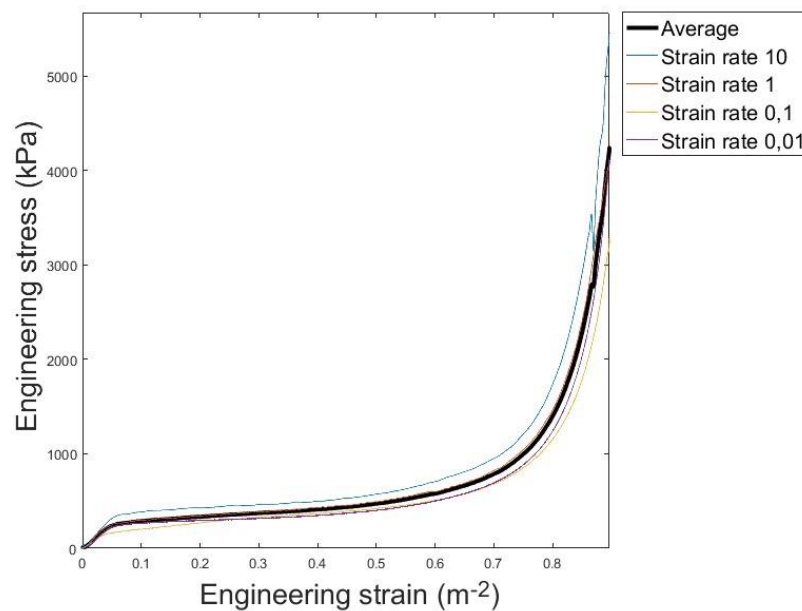


**Fig. 16:** Stress strain curves obtained after four strain rates were applied to the samples.

Fig. 17 shows the five curves obtained from the second test, when five specimens (belonging to different part of the foam of the helmet) were tested with the same applied strain rate of 10/s. They were also used to calculate an average stress-strain curve, which is the one that was used to implement the EPP properties into the FE model.

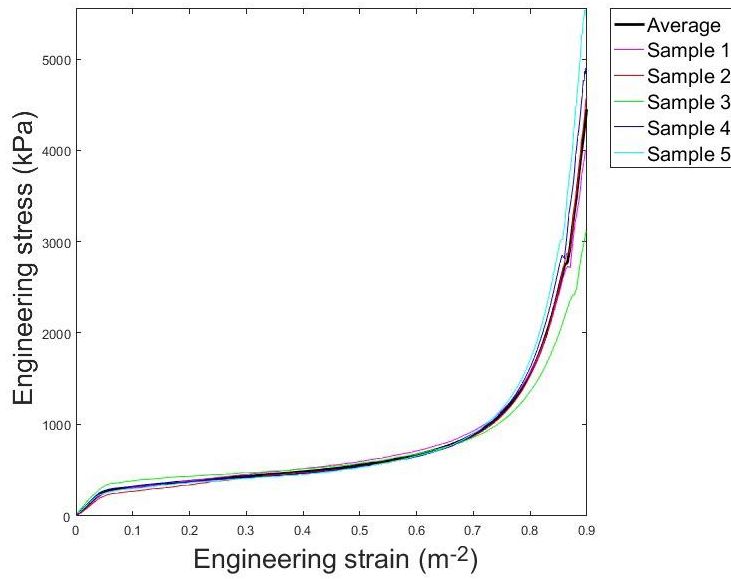


**Fig. 17:** Stress strain curves of the five samples and their average. . Ordinate values smaller than the peak value were not plotted.

From the curves shown in Fig. 17, five Young’s moduli were calculated by evaluating the gradient between the origin of the curve and where the plateau starts, as shown in Table 4. To have just one value to refer to, an average Young’s modulus was calculated: 5.2396531 MPa is the value that was used to implement the foam properties into the FE model.

**Table 4:** Young’s modulus of the five samples, with the correspondent height/diameter ratio

| Sample  | Stress (KPa) | Strain  | Height/diameter ratio | Young’s modulus (MPa) |
|---------|--------------|---------|-----------------------|-----------------------|
| 1       | 253.3        | 0.05335 | 1.333                 | 4.7478913             |
| 2       | 231.1        | 0.05672 | 1.458                 | 4,0744006             |
| 3       | 348          | 0.06069 | 1.333                 | 5.7340583             |
| 4       | 248.7        | 0.04077 | 1.350                 | 6.1000736             |
| 5       | 224.5        | 0.04051 | 1.333                 | 5.5418415             |
| AVERAGE |              |         |                       | 5.2396531             |

The density was calculated by dividing the mass of the specimen for its volume: the first was measured to be 0.008 g, while the radius of the samples was 6 mm. The final value, which was implemented into the FE model, was 0.0544 g/cm<sup>3</sup>.

The Poisson’s ratio was set close to zero, since the specimens showed an indiscernible horizontal deformation, when underwent a vertical compression, as it can be observed in Fig.18. In particular, the \*o63\_CRUSHABLE\_FOAM card was implemented with a value of 0.005 for the Poisson’s ratio.

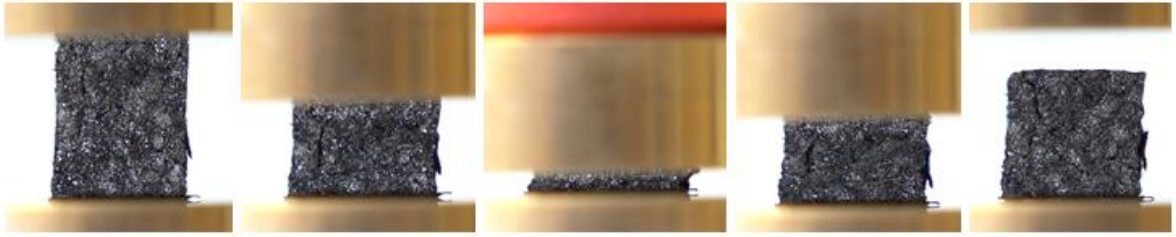


**Fig. 18:** Pictures taken with the Sony CyberShot DSC-RX10 II high speed camera during the compression of the specimens with the Instron Electropuls E3000 machine.

### 3.3 Simulation Results

The quantities obtained from the simulation results were the linear acceleration, the rotational velocity and the rotational acceleration recorded at the central node of the FE model of the accelerometer, positioned inside the FE model of the HIII form head.

The three quantities were measured for the three simulations with the two configurations, filtered with the SAE 300 low-pass digital filter and plotted against the experimental curves recorded by the nine accelerometers positioned inside the head form used to perform the drop tests [21].

#### 3.3.1. Results- First Configuration

The results of the Org 7538 Backward Impact simulation, the Org 7491 Lateral Impact simulation and the Org 7493 Pitched Impact simulation, obtained with the first configuration, are shown in Fig.19, Fig.20 and Fig.21 respectively. The simulation results are plotted in red against the laboratory drop test results in blue.

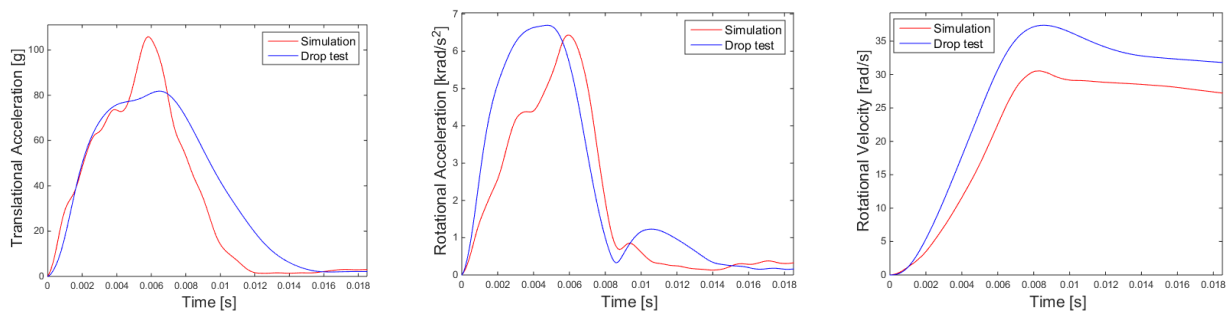


**Fig. 19:** Translational Acceleration (left), Rotational Acceleration (middle) and Rotational Velocity (right) of numerical simulation (red) and experimental drop test (blue) obtained during the Org 7538 Backward Impact with the first configuration.

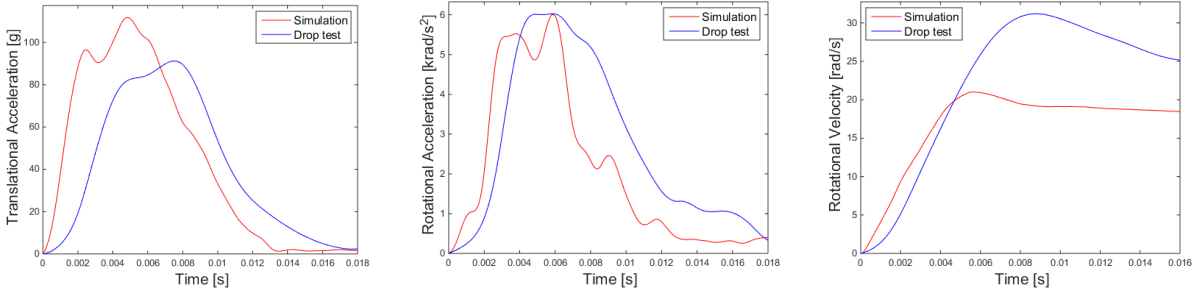


**Fig. 20:** Translational Acceleration (left), Rotational Acceleration (middle) and Rotational Velocity (right) of numerical simulation (red) and experimental drop test (blue) obtained during the Org 7491 Lateral Impact with the first configuration.

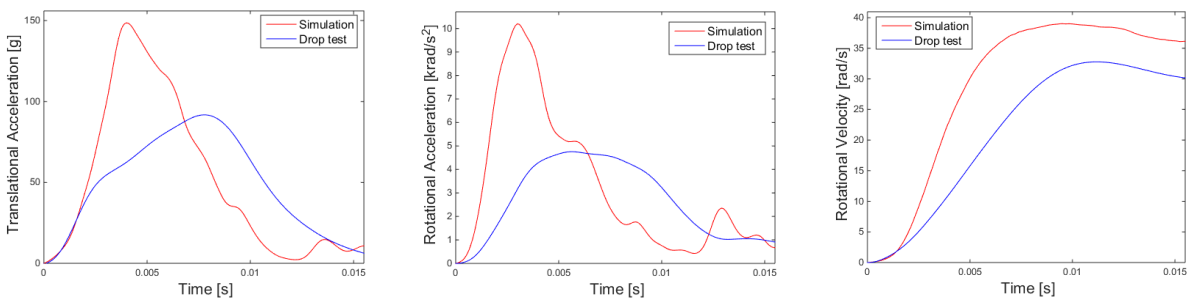


**Fig. 21:** Translational Acceleration (left), Rotational Acceleration (middle) and Rotational Velocity (right) of numerical simulation (red) and experimental drop test (blue) obtained during the Org 7493 Pitched Impact with the first configuration.

### 3.3.1.1 Correlation Coefficient

Table 5, Table 6 and Table 7 present the main results for the Org 7538, the Org 7491 and the Org 7493 respectively. The simulation results and the experimental results are compared in terms of peak values, times at which the peaks occur, the percentage of Peak Difference and the Pearson Coefficient calculated between the whole curves. The scatter diagrams (Fig.22) are provided only for the Org 7538 Backward Impact test, to show its correspondence with the Pearson Coefficients shown in Table 5.

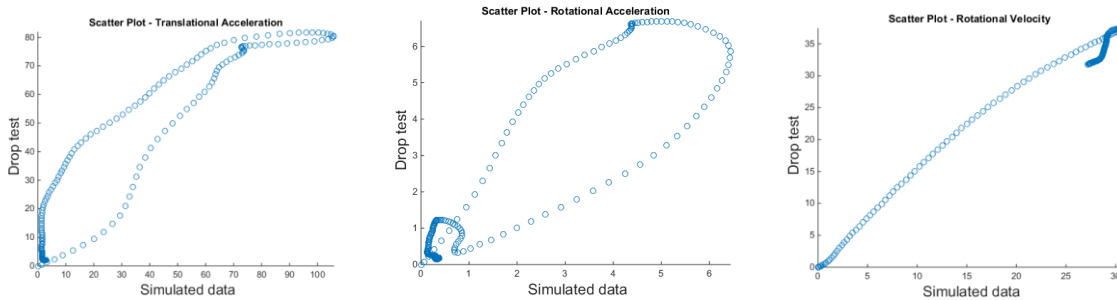


**Figure 22:** Scatter plots of: translational acceleration (left); rotational acceleration (middle) and rotational velocity (right) of the Org 7538 Backward Impact test simulated with the first configuration.

**Table 5:** Simulation and drop test results for the Org 7538 Backward Impact test with the first configuration.

| <b>Org 7538</b>                               | Data      | Peak Value | Time Peak [ms] | Pearson Coefficient ( <i>r</i> ) | Peak Difference [%] |
|---|-----------|------------|----------------|----------------------------------|---------------------|
| Translational Acceleration [g]                | SIM_data  | 105.82     | 5.8            | 0.9316                           | 29.31               |
|   | TEST_data | 81.83      | 6.5            |                                  |                     |
| Rotational Acceleration [rad/s <sup>2</sup> ] | SIM_data  | 6.43       | 5.9            | 0.8964                           | 4.03                |
|   | TEST_data | 6.7        | 4.8            |                                  |                     |
| Rotational Velocity [rad/s]                   | SIM_data  | 30.55      | 8.3            | 0.9889                           | 19.18               |
|   | TEST_data | 37.80      | 8.6            |                                  |                     |

**Table 6:** Simulation and drop test results for the Org 7491 Lateral Impact test with the first configuration.

| <b>Org 7491</b>                               | Data      | Peak Value | Time Peak [ms] | Pearson Coefficient ( <i>r</i> ) | Peak Difference [%] |
|---|-----------|------------|----------------|----------------------------------|---------------------|
| Translational Acceleration [g]                | SIM_data  | 111.82     | 4.8            | 0.7698                           | 20.36               |
|   | TEST_data | 91.21      | 7.5            |                                  |                     |
| Rotational Acceleration [rad/s <sup>2</sup> ] | SIM_data  | 6.01       | 5.9            | 0.8188                           | 0.16                |
|   | TEST_data | 6.02       | 5.9            |                                  |                     |
| Rotational Velocity [rad/s]                   | SIM_data  | 21.02      | 5.7            | 0.9074                           | 32.6                |
|   | TEST_data | 31.19      | 8.8            |                                  |                     |

**Table 7:** Simulation and drop test results for the Org 7493 Pitched Impact test with the first configuration.

| <b>Org 7493</b>                               | Data      | Peak Value | Time Peak [ms] | Pearson Coefficient ( <i>r</i> ) | Peak Difference [%] |
|---|-----------|------------|----------------|----------------------------------|---------------------|
| Translational Acceleration [g]                | SIM_data  | 148.57     | 4.0            | 0.6698                           | 61.92               |
|   | TEST_data | 91.75      | 7.8            |                                  |                     |
| Rotational Acceleration [rad/s <sup>2</sup> ] | SIM_data  | 10.2       | 3.0            | 0.4144                           | 114.28              |
|   | TEST_data | 4.76       | 5.6            |                                  |                     |
| Rotational Velocity [rad/s]                   | SIM_data  | 39.02      | 9.5            | 0.9516                           | 19.45               |
|   | TEST_data | 32.78      | 13.12          |                                  |                     |

### 3.3.1.2 Peak Linear Acceleration Score

The peak linear acceleration score was calculated for the three test designs, taking as TV the translational acceleration’s peak value from the test and as SV the one from the simulation. The score obtained for the backward impact was 70.88%, the one obtained for the lateral impact was 77.76%, while the pitched impact showed a score of 37.95%.

### 3.3.2 Results-Second Configuration

The results of the Org 7538 Backward Impact simulation, the Org 7491 Lateral Impact simulation and the Org 7493 Pitched Impact simulation, obtained with the second configuration, are shown in Fig.23, Fig.24 and Fig.25 respectively. The simulation results are plotted in red against the laboratory drop test results in blue.

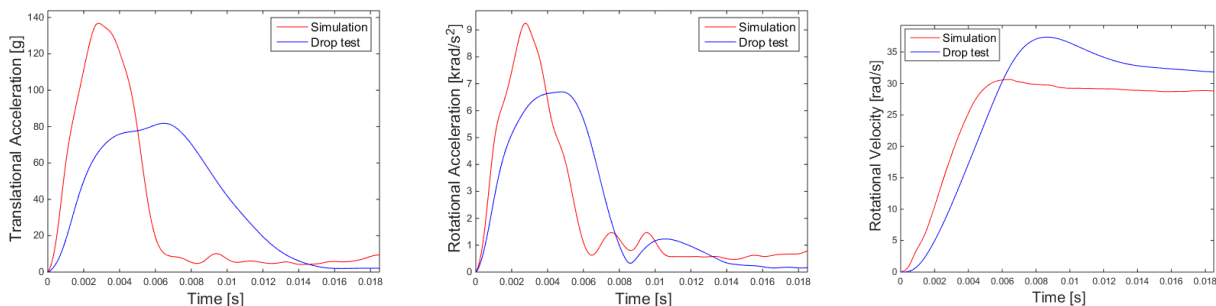


**Fig. 23:** Translational Acceleration (left), Rotational Acceleration (middle) and Rotational Velocity (right) of numerical simulation (red) and experimental drop test (blue) obtained during the Org 7538 Backward Impact with the second configuration.

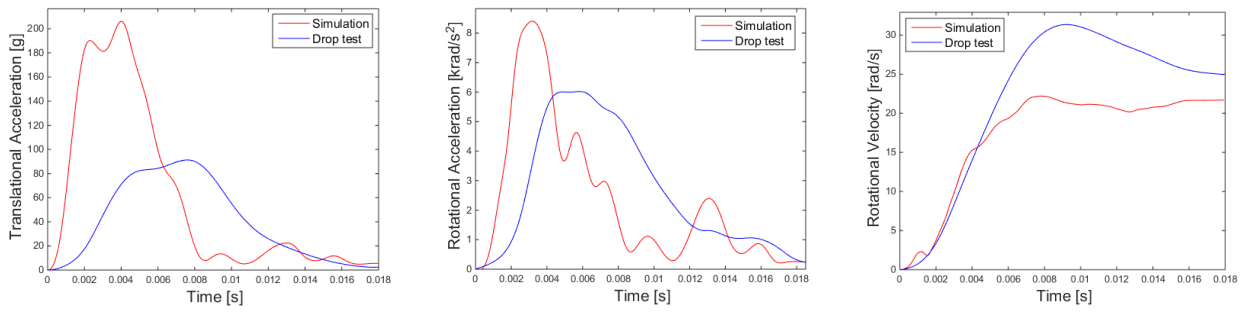


**Fig. 24:** Translational Acceleration (left), Rotational Acceleration (middle) and Rotational Velocity (right) of numerical simulation (red) and experimental drop test (blue) obtained during the Org 7491 Lateral Impact with the second configuration.

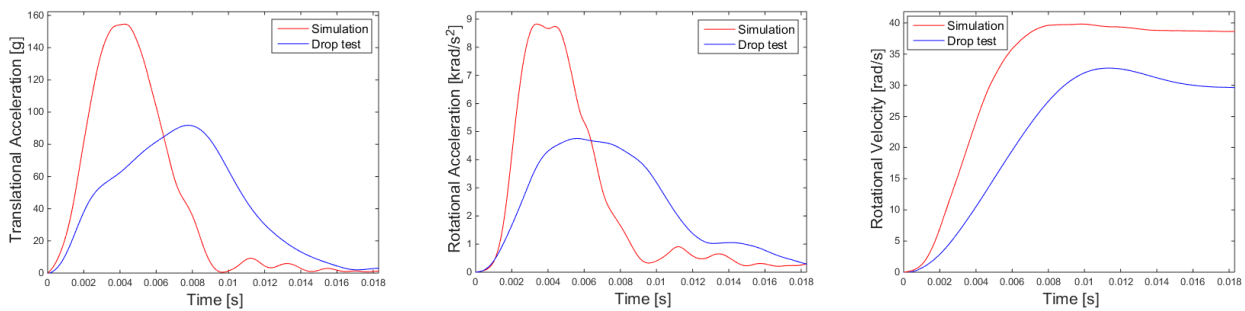


**Fig. 25:** Translational Acceleration (left), Rotational Acceleration (middle) and Rotational Velocity (right) of numerical simulation (red) and experimental drop test (blue) obtained during the Org 7493 Pitched Impact with the second configuration.

### 3.3.2.1 Correlation Coefficient

Table 8, Table 9 and Table 10 present the main results for the Org 7538, the Org 7491 and the Org 7493 respectively. As for the first configuration, the simulation results and the experimental results are compared in terms of peak values, times at which the peaks occur, the percentage of Peak Difference and the Pearson Coefficient calculated between the whole curves. The scatter diagrams (Fig.26) are provided only for the Org 7538 Backward Impact test, to show its correspondence with the Pearson Coefficients shown in Table 8.

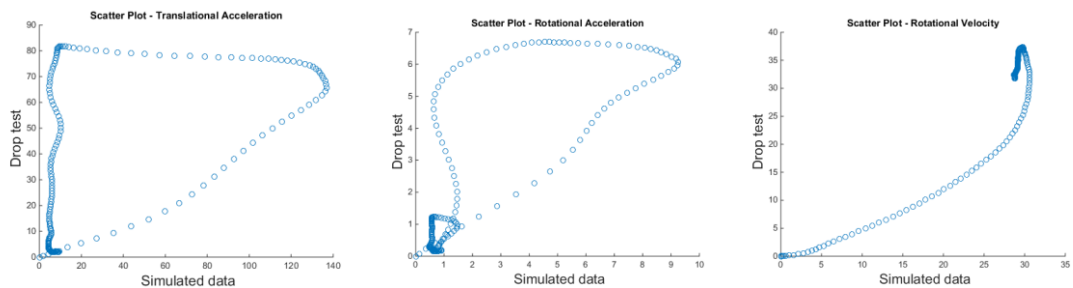


**Figure 26:** Scatter plots of: translational acceleration (left); rotational acceleration (middle) and rotational velocity (right) of the Org 7538 Backward Impact test simulated with the second configuration.

**Table 8:** Simulation and drop test results for the Org 7538 Backward Impact test with the second configuration.

| <b>Org 7538</b>                               | Data      | Peak Value | Time Peak [ms] | Pearson Coefficient ( <i>r</i> ) | Peak Difference [%] |
|---|-----------|------------|----------------|----------------------------------|---------------------|
| Translational Acceleration [g]                | SIM_data  | 136.89     | 2.8            | 0.5005                           | 67.28               |
|   | TEST_data | 81.83      | 6.5            |                                  |                     |
| Rotational Acceleration [rad/s <sup>2</sup> ] | SIM_data  | 9.25       | 2.8            | 0.7890                           | 38.05               |
|   | TEST_data | 6.7        | 4.8            |                                  |                     |
| Rotational Velocity [rad/s]                   | SIM_data  | 30.64      | 6.4            | 0.9315                           | 17.82               |
|   | TEST_data | 37.37      | 8.6            |                                  |                     |

**Table 9:** Simulation and drop test results for the Org 7491 Lateral Impact test with the second configuration.

| <b>Org 7491</b>                               | Data      | Peak Value | Time Peak [ms] | Pearson Coefficient ( <i>r</i> ) | Peak Difference [%] |
|---|-----------|------------|----------------|----------------------------------|---------------------|
| Translational Acceleration [g]                | SIM_data  | 206.32     | 4.0            | 0.3636                           | 126.12              |
|   | TEST_data | 91.24      | 7.6            |                                  |                     |
| Rotational Acceleration [rad/s <sup>2</sup> ] | SIM_data  | 8.41       | 3.2            | 0.4541                           | 39.7                |
|   | TEST_data | 6.02       | 5.8            |                                  |                     |
| Rotational Velocity [rad/s]                   | SIM_data  | 22.2       | 7.8            | 0.9679                           | 29.18               |
|   | TEST_data | 31.35      | 9.2            |                                  |                     |

**Table 10:** Simulation and drop test results for the Org 7493 Pitched Impact test with the second configuration.

| <b>Org 7493</b>                               | Data      | Peak Value | Time Peak [ms] | Pearson Coefficient ( <i>r</i> ) | Peak Difference [%] |
|---|-----------|------------|----------------|----------------------------------|---------------------|
| Translational Acceleration [g]                | SIM_data  | 154.56     | 4.3            | 0.5387                           | 68.45               |
|   | TEST_data | 91.75      | 7.8            |                                  |                     |
| Rotational Acceleration [rad/s <sup>2</sup> ] | SIM_data  | 8.83       | 3.4            | 0.6528                           | 77.41               |
|   | TEST_data | 4.96       | 5.6            |                                  |                     |
| Rotational Velocity [rad/s]                   | SIM_data  | 39.83      | 9.8            | 0.9477                           | 21.58               |
|   | TEST_data | 32.76      | 11.3           |                                  |                     |

### 3.3.1.2 Peak Linear Acceleration Score

The score obtained for the backward impact was 35.92%, the one obtained for the lateral impact was -19.81%, while the pitched impact showed a score of 30.76%.



## 4 Discussion

The quality of the FE model was checked twice: the second check was necessary not only to improve the quality of the model, but to create a model that could be easily used for running simulations with LS-DYNA. The removal of those element with DI smaller than 0.1 and of those with negative volume brought to the definition of a model which can still be improved, but can already be used to run stable simulations with LS-DYNA.

Among the parameters, those that do not meet the target were “Quad face min angle” and “Quad face max angle” for solid elements, since the percentage of failed elements were 2% and 3% respectively. The percentage (6%) of triangular elements that failed on the “Tria min angle” parameter is not to be considered, since it was evaluated in respect to the number of triangular shell elements (308), and not on the total. Although the quality target should be met by the 99% of the elements [29], this result is not alarming since the minimum and maximum angle of element faces do not affect the final results as much as a negative Jacobian value does. Improvements can still be achieved by a further cleaning and simplification of the geometry.

The first test conduct on the foam, which results are shown in Fig. 16, allowed to conclude that whether a static or a dynamic test was performed, it did not significantly influence the EPP characteristics. For this reason the Damping Coefficient was set to a low value in the definition of the foam in \*o63\_CRUSHABLE\_FOAM card. The curve corresponding to the sample 3 is the only one that differs from the others: a possible explanation for this could be that this part was more damaged than the others during the previous drop test, performed on the helmet at the MIPS.

The second experiment provided an average stress strain curve which is typical of foam behaviour and allowed a reliable implementation of the FE model of the foam. The Poisson's ratio was calculated with the combination of a ruler and video analysis: since the transverse deformation of the specimen was smaller than 0.001 m, the displacement detectable by the ruler, the Poisson's ratio was set to 0.005. The deformations occurred to the specimen are shown in Fig.18, where is clear that while the transverse deformation is not even detectable, the longitudinal one is more consistent, in accordance to the fact that EPP foam does not show complete

spring back after compression. Nevertheless, more specific video analysis techniques could be used to obtain more detailed results.

The curves obtained with the first configuration for the backward and the lateral tests (Fig. 19 and 20) had approximately the same shape and the time occurrence of the peak was less than 0.0027 s apart. Almost all the quantities registered for Org 7538 and Org 7491 showed a Pearson correlation coefficient bigger than 0.8, which indicated that the impact simulations were in good correlation with the drop tests [27]. The lowest Pearson coefficient values were registered in correspondence of the translational acceleration curves, fact that was further demonstrated by the low peak linear acceleration scores evaluated for both the impact scenarios. Good Pearson correlation coefficients were measured for rotational velocity, since they are both bigger than 0.9. Acceptable correlation coefficients were obtained for rotational acceleration in both cases, since they are almost 0.8. Low values were obtained for translational accelerations, which are further confirmed by the correspondent low peak linear acceleration scores and the high peak difference modulus. Even though the scatter plots of the translational and rotational acceleration (Fig.22, left and middle) do not show the desirable linear cloud of point lying on the diagonal (as shown in Fig.12), they correspond to a good Pearson coefficient: this is because the drop test and simulation curves have almost the same shape, but do change not only in time, but also in the ordinate value. In fact, the scatter plot of the rotational velocity looks more like a straight line because both the curves change at the same time and in only one direction, which means that they do not increase and decrease, but just increase.

Results from the Org 7493 were less reliable since a penetration occurred between the front foam and the front shell. This did not prevent the simulation from running, but produced trustworthy acceleration and velocity curves. To assess the reliability of the simulation, some parameters were checked: even though the energy ratio value was close to 1 and the kinetic and internal energies had a normal behaviour, the hourglass energy increased to more than 10% of the internal energy after 0.005 s (time at which the penetration occurred). Moreover, the sliding energies of the contacts between the external shell and the foam, the shell and the anvil, and the \*AUTOMATIC\_SINGLE\_SURFACE contact lost the symmetry after 0.005 s. The low level of reliability of the Org 7493 results was furthermore confirmed by the very low values of the Pearson correlation coefficient and the correlation coefficient. The time occurrence of the peak was more than 0.0048 s apart.

Nevertheless, the results of the first configuration meet those obtained in a similar study conducted on bicycle helmets [11], where not only a lower correlation was evaluated for the pitched impact but it was also found that pitched impact simulation overestimated the experimental rotational velocity. On the other hand, backward and lateral impact simulation were found to underestimate it, as it can be

seen in Fig. 19, 20 and 21. Another correlation between the results obtained in the article and those reported here is that the peaks of linear and rotational acceleration were more shifted in time -respect to those of the drop tests- for the pitched tests than for the other two.

On the other hand, the second configuration showed very low correlation scores, not only for the pitched impact but also for the lateral and especially for the backward impact. This produced the lowest  $r$  (0.3636) for the translational acceleration, while the only quantity with acceptable  $r$  was the rotational velocity, for all the three tests. This could be due to the fact that the shear-strain curve used was not derived from the EPP foam of the helmet, but was from an EPS sample. Moreover, a consistent movement of the head form model is recorded with the second configuration, which could have affected the results. Nonetheless, the computational time required by this configuration was almost half of the one required by the first configuration, indicating that the \*126\_MODIFIED\_HONEYCOMB could be a valid solution, after the contacts and the friction coefficients are clarified.

In general, the second configuration seems to overestimate the rotational and linear acceleration in all the three cases. Links to the article results [11] are found only for the rotational velocity, which is underestimated by the model for the backward and lateral impact, and overestimated in the pitched one.

The most reliable measured quantity was found out to be the rotational velocity, which gave very low peak difference percentages: for all the three impacts and for both the configurations it turned out to be the easiest quantity to reproduce.

The major limitations of this work concern the simulation set up. Firstly, an automatic fitting of the helmet model on the HIII should be performed by running a simulation where an appropriate \*INITIAL\_VELOCITY is applied to the helmet: in this way the head form will enter and then remain in contact with the foam as it happens in reality. This was avoided because a simulation at such a low velocity (10 cm/s) required more than 250 hours. In second place, it would have been appropriate not to change so many parameters between the first and the second configuration: if the same model would have been first tested with the \*063\_CRUSHABLE\_FOAM and then with the \*126\_MODIFIED\_HONEYCOMB, it would have been easier to decide for one or the other. Then, the number of contacts should be decreased to the minimum possible, in order to make the model more stable. In the end, more numerous and detailed analysis of the material would have allowed for a better characterization of the model.



## 5 Conclusion

A FE model of the Easton Synergy 380 ice-hockey helmet was created in HyperWorks, starting from a CAD file containing its geometry. The 2D and 3D meshes were checked to eliminate the elements with negative volume or DI smaller than 0.1. The EPP foam of the liner was tested in the laboratory to extrapolate its mechanical properties, such as the Young's modulus, the Poisson's ratio and the density. The latter were used to characterise the material model of the foam in Ls-Prepost. Three drop tests were simulated with two configurations and results analysed in terms of linear acceleration, rotational acceleration and rotational velocity. The correlation between experiments performed at the MIPS and numerical model was determined by evaluating the shape of the curves and the peak occurrence, the Pearson correlation coefficient and the peak linear acceleration. While the second configuration did not show promising results, the first one showed a good correlation for the backward and lateral impact, especially for the rotational velocity and acceleration. A lower correlation was calculated for the translational acceleration, since even the peak linear acceleration score was smaller than 80%. Although results from the pitched test were not completely reliable because of penetrations occurred during simulations, they were in agreement with those obtained from a previous study. Therefore it can be concluded that, even though a more detailed study of materials and a smarter definition of contacts could be performed, the work developed in this project represents a first attempt of a FE model validation and a first step towards the generation of a stable and reliable model, which could be coupled with a FE model of a head form to reproduce approval tests. Not only, after appropriate material tests are performed, different combination of foams can be evaluated in terms of absorbed energy and damping efficiency. Moreover, the helmet model can be coupled with the KTH Head and Neck model to analyse real game impacts and predict traumatic brain injuries [30].



# **APPENDIX A**

State of the Art



## Table of Contents

|   |           |
|---|-----------|
| <b>1 Sport-Related Traumatic Brain Injuries.....</b>  | <b>39</b> |
| 1.1 MILD TRAUMATIC BRAIN INJURIES.....                | 39        |
| 1.2 MILD TRAUMATIC BRAIN INJURIES IN ICE HOCKEY ..... | 40        |
| 1.3 HELMETS TO REDUCE SPORT-RELATED CONCUSSIONS ..... | 41        |
| <b>2 Helmet .....</b>                                 | <b>43</b> |
| 2.1 ROTATIONAL ACCELERATION .....                     | 43        |
| 2.2 HELMET PERFORMANCE EVALUATION .....               | 44        |
| <b>3 Finite Element Method .....</b>                  | <b>47</b> |
| 3.1 ADVANTAGES .....                                  | 48        |
| 3.2 DISADVANTAGES .....                               | 49        |
| <b>4 Recent Studies.....</b>                          | <b>51</b> |
| 4.1 ICE HOCKEY HELMET INVESTIGATIONS.....             | 51        |
| 4.2 HELMET FE MODELS .....                            | 52        |
| <b>5 Ideal Ice Hockey Helmet .....</b>                | <b>55</b> |
| <b>6 References .....</b>                             | <b>57</b> |



# 1 Sport-Related Traumatic Brain Injuries

## 1.1 Mild Traumatic Brain Injuries

Traumatic brain injuries (TBIs) are defined as a bump or jolt to the head that alter the normal function of brain tissue [3]. According to the Glasgow Coma Score, TBIs are divided into mild (15-13), moderate (12-9) and severe (8-3) [31]. A head injury can be categorised as a mild traumatic brain injury (mTBI) if one or more of the following situations occur: “confusion or disorientation, loss of consciousness for 30 minutes or less, post-traumatic amnesia for less than 24 hours, and/or other transient neurological abnormalities” [32]. Differences between severe and mild TBIs are shown in Fig.1.

TBIs can be further distinguished into focal and diffuse brain injuries. In focal injuries, a lesion causes local damage, which is visible without the aid of an instrument. Injuries that fall into this group are Subdural and Epidural Hematoma, contusions and Intracerebral Hematomas [7]. Diffuse head injuries are on the other hand those that involve mechanical mechanisms such as negative intracranial pressure and excessive shear strain: they are associated with general disruption of brain functioning and are invisible [4]. These can be categorised into concussion, Diffuse Axonal Injury (DAI) and brain swelling.

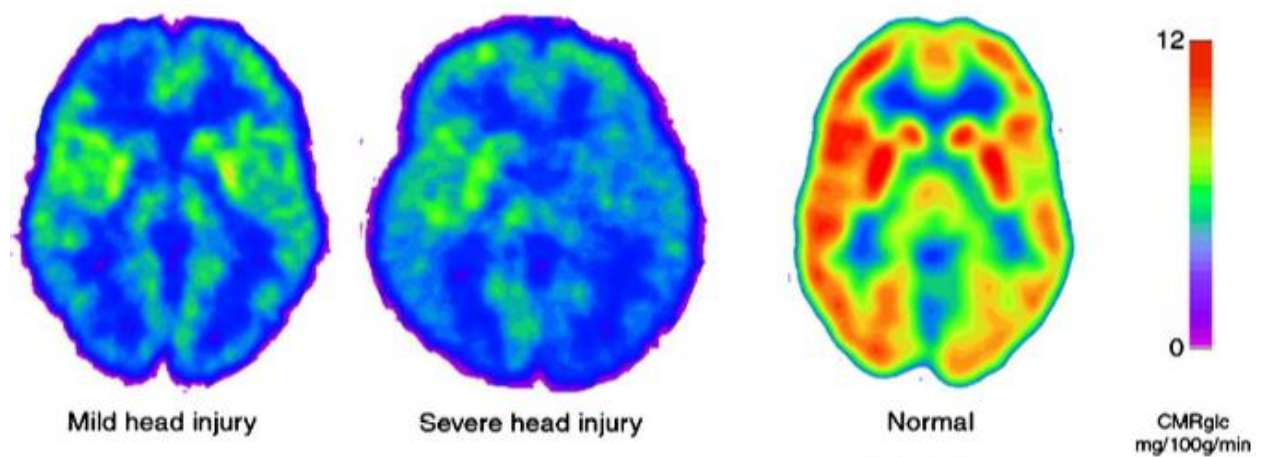


**Fig. 1:** PET images show the reduction of the glucose cerebral metabolic rate (CMRglc) after mild and severe TBIs [33]

Recent investigations have mainly focused on severe TBIs, even though mTBIs are known to be more than 10 times more prevalent [34]. Moreover, the possibility of recovery from mTBI is larger than from moderate and severe TBI. There are several cases where patients deal with everyday disabilities caused by mTBI. In fact most of the consequences of mTBI manifest many years after the trauma, and are therefore difficult to link to the initial injury, which patients may even seem to have completely recovered from [31]. Disorders related to attention, visual and working memory and executive functions are some of the consequences of mild head injuries, that makes TBIs responsible for what has been recognised to be “a longlife chronic health condition” [31].

What makes mTBIs dangerous is that neither their presence nor their relevance can be fully detected with conventional imaging techniques [35]. In a study conducted in 2001, only 77% of patients suffering from mTBIs showed abnormal findings either on SPECT scans or MR images. Although most of the patients with mTBIs presented abnormalities on neuroimages, the correlation between SPECT and MR results was poor. Moreover, once the neurocognitive performances were tested, no difference was found between patients who had normal and abnormal MR scans [36], this supporting the thesis concerning that mTBIs’ consequences become detectable years after the accident.

## **1.2 Mild Traumatic Brain Injuries in Ice Hockey**

MTBIs are the most recurrent in contact sports; in particular it has been reported that concussions are the most common head injuries among sport related TBIs [4], [37]. According to a recent article [3], 446.788 sport-related TBIs were registered in America in 2009 and this number represented an increase of 95.000 from the prior year. Relating to ice-hockey contribution, 8154 cases of TBIs are known to be recorded during the year. Researches analysing the cause of concussion-related TBIs in the National Hockey League demonstrated that only 7% of all concussions were caused by falls, while 88% were due to collisions between players; among this percentage, the most common events were shoulder-to-head impacts [10]. Examples of collisions in ice hockey are shown in Fig.2.



**Fig.2:** Examples of collisions in ice hockey.

The main difference between TBIs occurring in normal life and during sport activity is that the contribution from Second Impact Syndrome (SIS) has to be added, since the sportive gesture that causes the impact can be repeated during practices and games. SIS results from brain swelling occurring after a further concussion is sustained, before the player had the time to recover from a previous concussion [38]. After the second impact occurs, the athlete remains on his feet for 15-60 seconds; he usually walks off the playing court unassisted and then collapses to the ground, with respiratory failure and lack of eye movement [38]. Due to the nature of SIS definition, statistical data regarding the occurrence of SIS are very little [39], [40].

### **1.3 Helmets to Reduce Sport-Related Concussions**

George Owen was the first player to wear an ice hockey helmet in a regular match in 1928-1928, but only after 1933, when a player almost lost his life during a contact accident, some prototypes of helmet were proposed.

Helmets play a central role in providing protection to the players: it has been demonstrated that the use of helmets helps in reducing the impact incidence [4]. Each helmet is designed for the specific sport and the materials are chosen to minimise as much as possible the consequences of the collision to the brain. According to the type of injury the helmet is designed for, different principles should be applied [41]. To prevent the fracture of the skull, the head has to be protected from the penetration of sharp objects: for this reason the helmet's shell has to have an adequate strength. Diverse assumptions should be taken in order to prevent closed TBIs: both the shell and the liner are supposed to absorb most of the impact energy and distribute the mechanical wave over the helmet's surface, in

order not to create concentrate dynamic stress [4]. Generally, the principal aim is to maximise the impact energy absorption of the inner layer. The foam that composes the cushion layer is the part that absorbs the majority of the energy.

## 2 Helmet

### 2.1 Rotational Acceleration

Despite the introduction of helmets led to a reduction of skull fracture and focal brain injuries during sport activities, the number of concussions has not followed the same decreasing trend. This can probably be associated to the fact that helmets are designed to deal with linear acceleration, but not with rotational acceleration [41]–[43]. In fact rotationally-induced strains within the brain tissue, which have been proved to be connected to concussions, are not correlated to linear acceleration, but to rotational acceleration [8], [44].

The relationships describing the linear and angular velocity, and the linear and angular acceleration respectively, are shown below. The used parameters are: the displacement  $x$ , the velocity  $v$  and the linear acceleration  $a$ ; the angular displacement  $\theta$ , the angular velocity  $\omega$  and the angular acceleration  $\alpha$ .

$$\text{linear velocity} \quad v(t) = \frac{dx(t)}{dt} \quad ; \quad \omega(t) = \frac{d\theta(t)}{dt} \quad \text{angular velocity}$$

$$\text{linear acceleration} \quad a(t) = \frac{dv(t)}{dt} \quad ; \quad \alpha(t) = \frac{d\omega(t)}{dt} \quad \text{angular acceleration}$$

In recent years rotational acceleration has been taken into account in the evaluation of helmet performances. In a study about equestrian helmet, Forero Rueda et al. [8] underline the need to add rotational kinematics in the parameters considered for future helmets design. What was found is that a change in rotational acceleration reflects “the same change in injury-related loads to neural tissue such as stress or strain” better than linear acceleration does. Similarly, in [41] it is confirmed that diffuse brain injuries, such as concussion and DAI, are linked to rotational acceleration, instead of linear. It is also stated that Maximum Principal Strain (MPS) and Von Mises (VM) stress could be predicted more accurately from peak resultant angular acceleration than peak linear acceleration

## 2.2 Helmet Performance Evaluation

Helmets testing and impacts simulations are necessary to improve the design of the helmets to maximise their protective capacity. In order to increase the performances, it is necessary to understand where and why helmets fail in their protective function. The reconstruction of the accident is therefore an important tool to find out how the impact occurred [45], i.e. at which velocities and in which positions the two players impacted one another. Several techniques can be used to recreate the circumstances of the accident, moreover there is a high number of variables that need to be taken into account: high-speed camera documentations of the event and data about the victim and the occurred injury would be optimal [45]. For example, the location of the brain swelling can be a good indicator of where the energy impact was at its highest level. When the accident circumstances are understood, the impact simulation can be performed.

There are three main modes to simulate an impact: dummy – or Anthropometric Test Device (ATD)- simulations, Post Mortem Human Subject (PMHS) simulations and mathematical model simulations. Mathematical methods include human body modelling with lumped-mass models, rigid-body models or Finite Element (FE) models, as shown in Fig.3. Among these three methods, FE models represent the most reliable. Secondary methods are represented by human volunteers or animals simulations [45]. ATD and PMHS methods are briefly discussed in the following paragraphs, since helmet tests mainly rely on them [46].

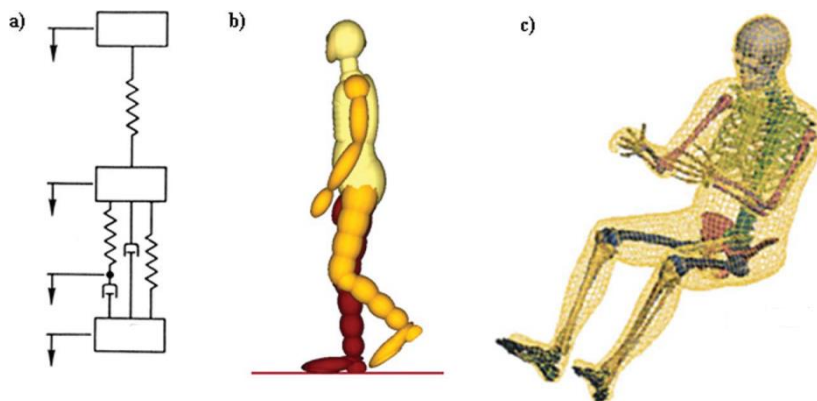


**Fig. 3:** Mathematical models: a) lumped-mass model of thorax; b) rigid-body model and c) FE model of human body [6].

ATD simulations make use of a manikin, also called dummy, which aims to reproduce the anthropometry of the human body or a part of it (see Fig.4 for examples). Since it is supposed to mimic also the structural response of the body, it is constructed with different materials (for examples foams, polymer composites

and metals) to imitate both the inner and external components of human body. Moreover, dummies are equipped with sensors, in order to measure forces, accelerations and displacements due to the impact [6]. Since ADTs are meant to be robust [45], although they show roughly the human anatomy, some parts of the head, such as the skull and the cerebrospinal fluid, are not present.



**Fig. 4:** Examples of dummies used in ATD simulations [6].

In PMHS simulations cadavers are used to reconstruct impacts. The most obvious advantage that PMHSs have is that all the human anatomical structures are fully represented. Nevertheless, the ability of mimicking the human response does not depend only on the geometry of the structures, but also on the properties of tissue and on the physiological response. In relation to this point, some important issues of PMHS are that they lack muscle tension and that fluids and gasses are altered because of the decomposition of the body. Moreover the presence of rigor mortis causes tissue rigidity and limits the window of time for investigations [6]. Furthermore, cadavers experiments are more time and money consuming than correspondent dummy experiments.

Dummies and PMHSs simulations can be used to investigate the helmet strength by reproducing plausible accidents. Several variables can be addressed to the simulation, such as velocities and angles of the structures impacting one another, and numerical quantities can be recorded to evaluate

the helmet performances, such as linear and rotational acceleration [47]. Although the basic requirement for a helmet to pass the pass/fail criteria is that linear acceleration is kept within the range of 250-300 g [48], concussion may already have occurred before the helmet strength reaches its ultimate level. Moreover, because of their lack of biofidelity, these methodologies do not provide reliable information about brain tissue conditions, such as stress/strain level and the intracranial pressure [4].

FE models can be used to overcome the limitations listed above: a proper FE model is able to reproduce not only the anatomy and the anthropometry of the head, but also the biological response of the brain tissue. By combining a head FE model and a helmet FE model, it is possible to measure quantities such as HIC value [49], head impact power (HIP) value [44], VM shear stress and brain pressure [50], which are good indicators of the TBI's severity.

### 3 Finite Element Method

The FE method is a numerical method commonly used in engineering to deal with complex problems, which are difficult to be solved analytically. It allows the user to obtain accurate approximations of partial differential equations (PDEs) solutions [51].

The subject is subdivided into small elements, which are connected through nodes to create a mesh [51]. Each element is characterised by its own assortment of shape functions. When the solid body model deforms, because of external forces, nodes move to new positions. Shape functions and nodal displacements are the starting point to approximate the solution of PDEs.

By dividing the original structure in small sections, the continuous system is discretised and the degrees of freedom (DOFs) turn into finite in the system. Principles, characteristics and physical laws can then be applied to the elements and the governing PDEs are automatically defined for each element and recombined into a global system of equations [51], which can then be solved by implicit or explicit integration methods.

The elements can vary in number, shape and dimension according to the geometry that need to be modelled, the type of analysis that has to be performed, the accuracy and results that are desired and the available computational power. To solve one dimension problems line segments can be used. On the other hand, 2D and 3D problems are resolved in form of shell and solid. In this case, elements shape can vary from triangles, quadrilaterals, tetrahedrons and hexahedrons. Since no gap or overlapping can be present between elements, mixed meshes of triangular and quadrilateral elements are often used to overcome this problem [51]. Even if triangular elements are less accurate than quadrilaterals, they are used quite often because of their adaptability to complex geometry: they are widely present in geometry with acute corners; quadrilaterals are used especially in those parts where a high level of accuracy is required [52].

Regarding the specific case of the FE modelling a helmet, the exterior plastic layer is treated as a 2D shell, while the inner foam liner is modelled as a solid. Although no real life structure is truly 2D, many 3D practical problems are idealized in two dimensional problems, in order to reduce the computational time for simulations: using 3D elements to shape the entire problem leads to an enormous number of DOFs [53]. A 3D structure such as the shell of the helmet can be modelled as a 2D problem as long as one of the three dimensions is appreciably smaller than the other two. The interior foam is modelled with 3D elements and treated as a normal solid structure. In Fig. 5 two different helmets FE models are shown, to reveal the similarities between them.

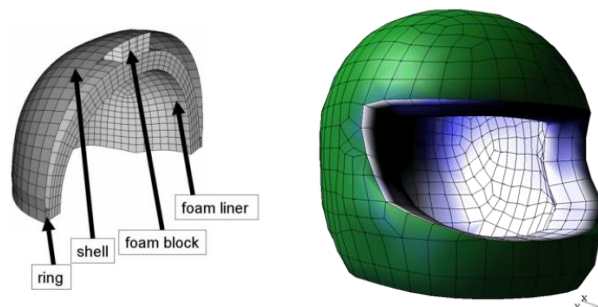


**Fig. 5:** FE model of equestrian helmet (left) [8] and of motorcycle helmet (right); the shell and the liner are modelled separately.

### 3.1 Advantages

In contrast to simulations with dummies and PMHS, FE model can give physiological responses. If the model is developed with high number of details it can provide important information such as muscle activation and deformation of human tissue, and it can predict injury [45]. Regarding the helmets FE models, they are able to measure quantities such as VM stress, longitudinal strain [8], rotational and linear acceleration [9] and impact duration [10]. Moreover, FE simulations are repeatable and reproducible: if coupled with a head FE model, FE helmet simulations can be considered experiments without biological variability [7]. Additionally, several material models are available to define the properties of the different parts of the helmet, such as the shell and the liner. Another advantage offered by this method is that it allows the user to analyse and solve the problem interacting through a graphic interface, which makes the understanding of the problem easier.

### 3.2 Disadvantages

Although the computational power has increased, with consequently increase of the usage of numerical models, studies with FE models still remain few. The reason lies in the fact that FE simulations need more computational time than, for example, rigid body simulations, which are even easier to reposition. If the problem is a 3D domain, each element is represented by three DOFs, which means: given  $n_d$  the number of nodes of the model and  $n_f$  the number of DOFs of each element,  $n_d \times n_f$  is the total amount of DOFs of the whole model. Considering that FE helmet models can be even composed by 14.000 elements [9], the considering computational power that is required is evident. Furthermore, since the number of elements increase with the increment of the level of accuracy required, the time necessary to perform a FE simulation increases with the accuracy of the model [45].

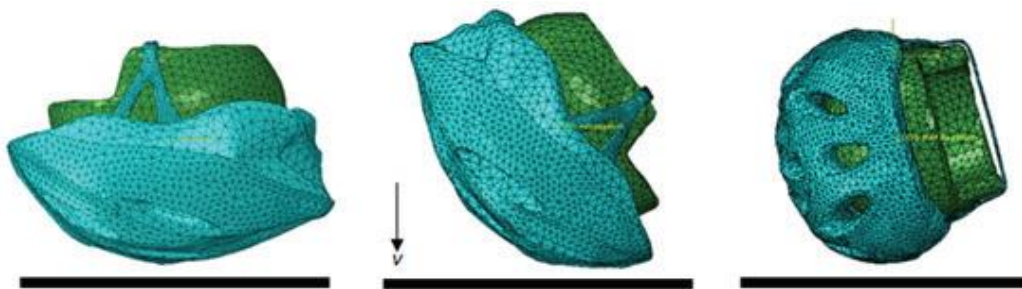


**Fig. 6:** A FE simulation of three impact positions for a bicycle helmet [27]



## 4 Recent Studies

### 4.1 Ice Hockey Helmet Investigations

Several studies have recently been conducted on ice hockey: some of those being statistical researches about different aspects of the sport, while others represent detailed analysis of helmet performances.

Tegner et al. [5] calculated the frequency of concussion in ice hockey in Sweden, with the help of questionnaires filled by players and doctors. The results led to the alarming conclusion that 20% of Swedish players are likely to experience at least one concussion during their careers. Moreover, two periods of six years (1996-2001 and 2002-2007) were compared in terms of the number of concussions and the recovery time for players. What was found is that although the rate of concussions was almost constant, the number of players returning to play (after the injury) decreased and players were absent from games longer, which means that the management of concussion was more conservative [43].

Two similar studies were conducted to find out the connection between linear and rotational acceleration and the brain injury risk. In the oldest study, a helmeted Hybrid III headform is impacted in five different impact sites during laboratory tests; the measured accelerations are used to run the University College Dublin Brain Trauma Model (UCDBTM), which is a FE model of the head and its components. By analysing the stresses and strains in the brain predicted by the model, it is evident that the risk of injury is present even at those low linear accelerations that would pass standard safety certifications [41]. In the more recent research, ten helmets are tested in the same way: an ice hockey accident is reconstructed in laboratory; impact parameters are obtained through video analysis; linear and rotational accelerations are calculated with mechanical methods; the two quantities are used as input to UCDBTM. What turns out is that although the magnitude of strain is not completely represented by the accelerations, both of them are fundamental to the evaluation of the helmets [54][54].

A research on the efficiency of the foams used for the liner was conducted in Canada. Vinyl nitrile (VN) liner and expanded polypropylene (EPP) liner are tested through physical tests: a helmeted Hybrid III headform is impacted using a pneumatic linear impactor. By measuring HIC value and peak linear and angular acceleration, it is possible to state that while EPP foam liner helmets reduce linear acceleration, VN decreases angular acceleration. Moreover, it is stated that the impact location affects the performances of the liner [47].

## 4.2 Helmet FE Models

Some examples of already developed FE models of sport helmets are presented in the following paragraphs, to highlight the purposes for which a FE model can be used.

In [8] a FE model of an equestrian helmet is created in order to demonstrate that linear acceleration is not a sufficient parameter to establish the severity of the brain injury. In the study, FE simulations are used to compare two different ways of testing a helmet: standard helmeted rigid headform impact simulations against helmeted-head model UCDBTM. The level of correlation between linear and rotational acceleration (measured in FE headform simulations) and stress and strain in the brain (measured in FE UCDBTM simulations) are studied. What is found is that a reduction in helmet's linear acceleration does not correspond to a reduction in the level of stress/strain in the brain tissue, which are responsible for brain injuries. In parallel, it was noticed that the correlation between linear acceleration and the severity of brain injury depends on the site of the impact. This allowed the author to conclude that rotational acceleration should have been used to evaluate the level of stress and strain in the brain, since it encompasses human head sensitivity to different directional impacts.

Some studies have been conducted to analyse the protective capacity of motorcycle helmets. Afshari et al. [49] used a FE model of a helmet to compare helmeted and unhelmeted impacts. Parameters such as HIC value, pressure in the brain, stress and strain in brain tissue and velocity changes were considered to evaluate the differences between the two impacts. The resulting severity of injury showed a wide variation between the two cases, which led to the conclusion that helmet reduces a lot the probability of injury. Moreover, it is stated that a proper FE model of the helmet and the head can help in evaluation of helmets performances. A second study on motorcycle helmets tested different materials combinations: a carbon-fiber shell is compared to a glass-fiber and a Kevlar-fiber shell. A general FE model of the shell/liner/headform complex is created and then three different material properties are applied to the shell. Drop tests are simulated and the maximum

acceleration measured at the headform's centre of gravity and the maximum value of HIC are taken into account. According to the value of these parameters, the Kevlar shell resulted to be the best in terms of reducing the stress and strain in the brain [9].

The good correlation between FE and physical simulation has been confirmed in a study on bicycle helmets [27]. Laboratory drop tests and FE simulations of drop tests are performed on three different bicycle helmets and three correlation methods are carried out to evaluate the correspondence between physical and numerical experiments: peak linear acceleration on three impact locations, impact duration and Pearson correlation coefficient are considered for each helmet. What is concluded is that the numerical model provides results in accordance to those provided by physical tests.



## 5 Ideal Ice Hockey Helmet

Although the ideal ice hockey helmet is that which protects players totally, it has been assessed that no helmet can give complete protection from head injuries and that the risk associated with this sport is always present [4], [55]. Nevertheless, there are some important aspects that can be taken into account to increase the protective capacity of a helmet. The basic requirement for a helmet is that the acceleration peaks are in the range of 250-300 g [48], despite this is not the only parameter that should be considered. First of all, the level of stress concentration should be minimized at the contact point, the absorbed portion of mechanical energy due to the impact needs to be maximised, the impact impulse duration has to be increased as much/far as possible. In general, the helmet should be able to change the energy level and the pattern of mechanical wave [4].

The main protective components of an ice hockey helmet are the shell and the liner. The stiffness of the exterior shell is fundamental to both prevent sharp object to penetrate the helmet and to diversify the impact pressure on a larger area of the brain tissue [4]. In a study on motorcycle helmets, it has been observed that deformable shells give more protection against flat surfaces, while stiff shells protection is more effective against round surfaces. That is because the load spreading area increases with the increase of the shell stiffness [56]. Moreover, the shell can absorb part of the impact energy through plastic deformation, by changing kinetic energy to heat [57].

On the other hand, the inner liner is expected to further absorb the energy of the impact and to make the pressure impact last longer. Expanded Polystyrene (EPS) and EPP are the components commonly used for helmet foam liners [48]. The most typical mode of deformation among foams is by compression. The stress-strain curve of foam can be divided into three zones: a linear elastic phase, a linear plastic phase and a densification phase, as shown in Fig.7. During the first stage the material re-acquires its original properties and shape once the load is removed. The second phase, which is characterised by a flat plateau, is the most crucial as the foam absorbs most of the mechanical energy, which is why it is desirable that this phase is longer. In this phase the gaseous component of the foam is affected: the gas can either exit the foam through pores or channels or be compressed, in open cell foams and closed cell foams respectively [58]. This leads to a permanent rupture of the cells and an irreparable damage to the foam. The last phase

corresponds to the total fracture, immediately after the material reaches its ultimate tensile stress.

A way to overcome the irreparability of EPS first damage is actually a subject of study. In one study a micro-agglomerate cork (MAC) padding is proposed and analysed, since it is a viscoelastic material with a good ability to absorb energy and to almost totally spring back. What has been found is that although MAC liner could overcome this obstacle, it would increase the helmet weight and the peak acceleration value. Thus EPS liner are confirmed to be better in yielding in a first impact, in terms of head acceleration [59]. A similar research was conducted to evaluate the performances of an aluminium honeycomb reinforced liner. The helmet prototype is tested in terms of HIC value and peak linear acceleration. The results show that the prototype gives better performance than its commercial counterpart when tested against the kerbstone anvil; some improvements, although limited, are registered for impacts against the flat anvil [56].

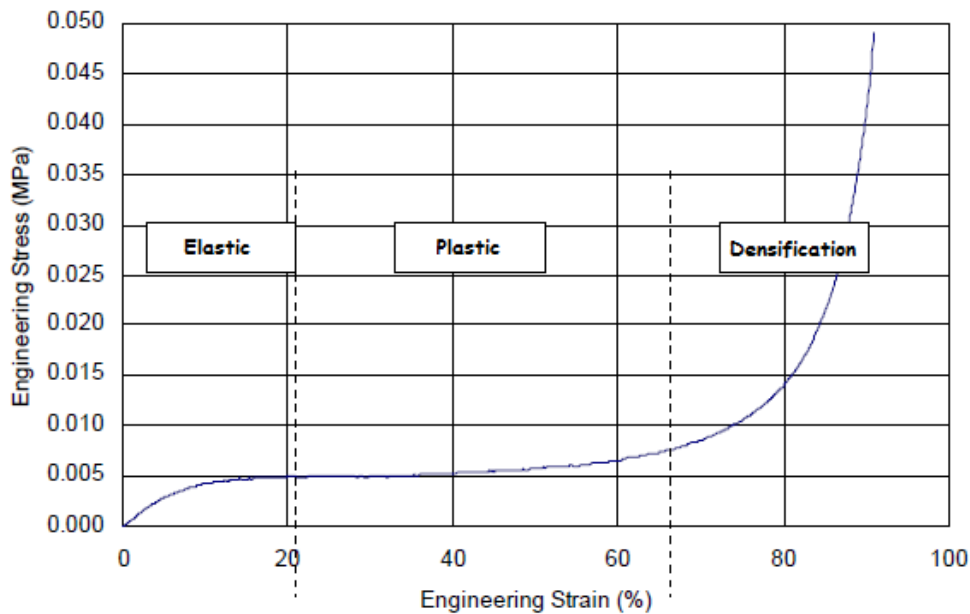


**Fig. 7:** Typical stress-strain curve of foam (Modified by [58])

## 6 References

- [1] B. W. Benson, M. S. Rose, and W. H. Meeuwisse, "The impact of face shield use on concussions in ice hockey: a multivariate analysis.," *Br. J. Sports Med.*, vol. 36, no. 1, pp. 27–32, 2002.
- [2] C. Asplund, S. Bettcher, and J. Borchers, "Facial protection and head injuries in ice hockey: a systematic review.," *Br. J. Sports Med.*, vol. 43, no. 13, pp. 993–999, 2009.
- [3] BMA, "Traumatic Brain Injury," vol. 2007, no. 12/28/2007. .
- [4] Y. Luo and Z. Liang, "Sport helmet design and virtual impact test by image-based finite element modeling," *Conf. Proc. ... Annu. Int. Conf. IEEE Eng. Med. Biol. Soc. IEEE Eng. Med. Biol. Soc. Annu. Conf.*, vol. 2013, pp. 7237–7240, 2013.
- [5] Y. Tegner and R. Lorentzon, "Concussion among Swedish elite ice hockey players," *Br J Sport. Med*, vol. 30, no. 3, pp. 251–255, 1996.
- [6] J. R. Crandall *et al.*, "Human surrogates for injury biomechanics research," *Clin. Anat.*, vol. 24, no. 3, pp. 362–371, 2011.
- [7] S. Kleiven, "Finite Element Modeling of the Human Head," *Med. Biol. ....*, vol. 12, no. 1, pp. 14–21, 2002.
- [8] M. a Forero Rueda, L. Cui, and M. D. Gilchrist, "Finite element modelling of equestrian helmet impacts exposes the need to address rotational kinematics in future helmet designs.," *Comput. Methods Biomech. Biomed. Engin.*, vol. 14, no. 12, pp. 1021–31, 2011.
- [9] V. Kostopoulos, Y. P. Markopoulos, G. Giannopoulos, and D. E. Vlachos, "Finite element analysis of impact damage response of composite motorcycle safety helmets," *Compos. Part B*, vol. 33, no. 2, pp. 99–107, 2002.
- [10] J. M. Clark, A. Post, T. B. Hoshizaki, and M. D. Gilchrist, "Protective Capacity of Ice Hockey Helmets against Different Impact Events," *Ann. Biomed. Eng.*, vol. 44, no. 12, pp. 3693–3704, 2016.
- [11] M. Fahlstedt, P. Halldin, and S. Kleiven, "The protective effect of a helmet in three bicycle accidents - A finite element study," *Accid. Anal. Prev.*, vol. 91, pp. 135–143, 2016.
- [12] "Large Model Finite Element Preprocessing | Altair HyperMesh." [Online]. Available: <http://www.altairhyperworks.com/product/HyperMesh>. [Accessed: 22-May-2017].
- [13] A. Engineering, "When to Use 2-D Elements Family of 2-D elements," 2012.
- [14] "Making a Solid Mappable." [Online]. Available: [https://connect.altair.com/CP/SA/training/self\\_paced/aero\\_v13/content/chapter6/ch2s2\\_mappable\\_text.htm](https://connect.altair.com/CP/SA/training/self_paced/aero_v13/content/chapter6/ch2s2_mappable_text.htm). [Accessed: 22-May-2017].
- [15] M. M. A. Vrijhoef and F. C. M. Driessens, "On the interaction between specimen and testing machine in mechanical testing procedures," *J. Biomech.*, vol. 4, no. 4, pp. 233–238, 1971.
- [16] G. M. Pharr, W. C. Oliver, and F. R. Brotzen, "On the generality of the relationship among contact stiffness, contact area, and elastic-modulus during indentation," *J. Mater. Res.*, vol. 7, no. 3, pp. 613–617, 1992.

- [17] G. N. Greaves, A. L. Greer, R. S. Lakes, and T. Rouxel, "Poisson's ratio and modern materials," *Nat. Mater.*, vol. 10, no. 12, pp. 986–986, 2011.
- [18] "LS-PrePost Online Documentation | Overview." [Online]. Available: <http://www.lstc.com/lsp/overview.shtml>. [Accessed: 19-May-2017].
- [19] "LS-PrePost Online Documentation | Index." [Online]. Available: <http://www.lstc.com/lsp/>. [Accessed: 19-May-2017].
- [20] D. S. Liu, C. Y. Chang, C. M. Fan, and S. L. Hsu, "Influence of environmental factors on energy absorption degradation of polystyrene foam in protective helmets," *Eng. Fail. Anal.*, vol. 10, no. 5, pp. 581–591, 2003.
- [21] "MIPS Approval test method – version November 2015 Introduction KTH FE-Head Model," no. November, pp. 2–5, 2015.
- [22] A. King, "Measurement of Angular Acceleration of a Rigid Body Using Linear Accelerometers," no. September 1975, pp. 552–556, 2017.
- [23] H. J. Mertz and A. L. Irwin, "and Injury Risk Assessments," 2015.
- [24] P. Taylor, M. Aare, and P. Halldin, "A New Laboratory Rig for Evaluating Helmets Subject to Oblique Impacts A New Laboratory Rig for Evaluating," no. November 2013, pp. 37–41, 2010.
- [25] "Steels, General Properties." [Online]. Available: <http://www.matweb.com/search/datasheet.aspx?bassnum=MS0001&ckck=1>. [Accessed: 23-May-2017].
- [26] "MATLAB - Il linguaggio del calcolo tecnico." [Online]. Available: <https://it.mathworks.com/products/matlab.html>. [Accessed: 25-May-2017].
- [27] H. Mustafa, T. Y. Pang, T. Perret-Ellena, and A. Subic, "Finite Element Bicycle Helmet Models Development," *Procedia Technol.*, vol. 20, no. July, pp. 91–97, 2015.
- [28] V. Bewick, L. Cheek, and J. Ball, "Statistics review 7: Correlation and regression.," *Crit. Care*, vol. 7, no. 6, pp. 451–459, 2003.
- [29] F. S. Gayzik, D. P. Moreno, N. A. Vavalle, A. C. Rhyne, and J. D. Stitzel, "Development of a Full Human Body Finite Element Model for Blunt Injury Prediction Utilizing a Multi-Modality Medical Imaging Protocol," *12th Int. LS-DYNA Users Conf.*, no. December 2014, pp. 1–14, 2012.
- [30] S. Kleiven, "Predictors for traumatic brain injuries evaluated through accident reconstructions.," *Stapp Car Crash J*, vol. 51, no. October, pp. 81–114, 2007.
- [31] R. Diaz-Arrastia and P. E. Vos, "The clinical problem of traumatic head injury," *Trauma. Brain Inj.*, 2015.
- [32] L. J. Carroll, J. D. Cassidy, L. Holm, J. Kraus, and V. G. Coronado, "Methodological issues and research recommendations for mild traumatic brain injury: The WHO Collaborating Centre Task Force on mild Traumatic Brain Injury," *J. Rehabil. Med.*, vol. 36, no. SUPPL. 43, pp. 113–125, 2004.
- [33] J. P. Difiori and C. C. Giza, "<New Techniques in Concussion Imaging.pdf>," vol. 90095, pp. 35–39, 2010.

- [34] J. J. Bazarian, J. McClung, M. N. Shah, Y. Ting Cheng, W. Flesher, and J. Kraus, "Mild traumatic brain injury in the United States, 1998–2000," *Brain Inj.*, vol. 19, no. 2, pp. 85–91, 2005.
- [35] P. E. Vos, C. Marquez, D. Plata, and R. Diaz-arrastia, "Chapter 2 Neuroimaging in traumatic brain injury," *Trauma. Brain Inj.*, pp. 13–42, 2015.
- [36] P. A. Hofman, S. Z. Stapert, M. J. van Kroonenburgh, J. Jolles, K. J. de, and J. T. Wilmink, "MR imaging, single-photon emission CT, and neurocognitive performance after mild traumatic brain injury," *AJNR Am.J Neuroradiol.*, vol. 22, no. 3, pp. 441–449, 2001.
- [37] M. W. Report, "Centers for Disease Control & Prevention ( CDC ) Sports-Related Recurrent Brain Injuries — United States Published by : Centers for Disease Control & Prevention ( CDC ) Stable URL : <http://www.jstor.org/stable/23307480>," vol. 46, no. 10, pp. 224–227, 2017.
- [38] A. P. Bowen, "Second impact syndrome: A rare, catastrophic, preventable complication fo concussion in young athletes," *J. Emerg. Nurs.*, vol. 29, no. 3, pp. 287–289, 2003.
- [39] N. M. Wetjen, M. A. Pichelmann, and J. L. D. Atkinson, "Second impact syndrome: Concussion and second injury brain complications," *J. Am. Coll. Surg.*, vol. 211, no. 4, pp. 553–557, 2010.
- [40] R. W. Byard and R. Vink, "The second impact syndrome," *Forensic Sci. Med. Pathol.*, vol. 5, no. 1, pp. 36–38, 2009.
- [41] A. Post, A. Oeur, B. Hoshizaki, and M. D. Gilchrist, "Examination of the relationship between peak linear and angular accelerations to brain deformation metrics in hockey helmet impacts.," *Comput. Methods Biomech. Biomed. Engin.*, vol. 5842, no. October 2012, pp. 37–41, 2011.
- [42] R. a Wennberg and C. H. Tator, "National Hockey League reported concussions, 1986-87 to 2001-02," *Can. J. Neurol. Sci.*, vol. 30, no. 3, pp. 206–209, 2003.
- [43] I. R. Casson, D. C. Viano, J. W. Powell, and E. J. Pellman, "Twelve years of national football league concussion data.," *Sports Health*, vol. 2, no. 6, pp. 471–83, 2010.
- [44] S. Kleiven, "Evaluation of head injury criteria using a finite element model validated against experiments on localized brain motion, intracerebral acceleration, and intracranial pressure," *Int J Crashworthines*, vol. 11, no. 1, pp. 65–79, 2006.
- [45] M. Fahlstedt, *Numerical accident reconstructions: a biomechanical tool to understand and prevent head injuries*, no. 2015:4. 2015.
- [46] I. P. Fulfillment, A. Giacomazzi, C. Member, and C. Member, "Analysis of the Impact Performance of Ice Hockey Helmets," vol. 6, no. 4, pp. 1–7, 2008.
- [47] P. Rousseau, A. Post, and T. B. Hoshizaki, "The effects of impact management materials in ice hockey helmets on head injury criteria," *Proc. Inst. Mech. Eng. Part P J. Sport. Eng. Technol.*, vol. 223, no. 4, pp. 159–165, 2009.
- [48] L. Andena, F. Caimmi, L. Leonardi, A. Ghisi, S. Mariani, and F. Braghin, "Towards Safer Helmets: Characterisation, Modelling and Monitoring," *Procedia Eng.*, vol. 147, pp. 478–483, 2016.
- [49] A. Afshari and S. M. Rajaai, "Finite element simulations investigating the role of the helmet in reducing head injuries," *Int. J. Simul. Model.*, vol. 7, no. 1, pp. 42–51, 2008.

- [50] C. Deck, R. Willinger, and D. Baumgartner, "Helmet optimisation based on head-helmet modelling," *Comput. Aided Optim. Des. Struct. VIII*, vol. 13, pp. 319–328, 2003.
- [51] G. R. Liu, S. S. Quek, G. R. Liu, and S. S. Quek, "Chapter 3 – Fundamentals for Finite Element Method," in *The Finite Element Method*, 2014, pp. 43–79.
- [52] G. R. Liu, S. S. Quek, G. R. Liu, and S. S. Quek, "Chapter 7 – FEM for Two-Dimensional Solids," in *The Finite Element Method*, 2014, pp. 161–217.
- [53] G. R. Liu, S. S. Quek, G. R. Liu, and S. S. Quek, "Chapter 11 – Modeling Techniques," in *The Finite Element Method*, 2014, pp. 301–345.
- [54] R. Ouckama and D. J. Pearsall, "IRC-14-16 IRCOBI Conference 2014," pp. 72–80, 2014.
- [55] B. Rowson, S. Rowson, and S. M. Duma, "Hockey STAR: A Methodology for Assessing the Biomechanical Performance of Hockey Helmets," *Ann. Biomed. Eng.*, vol. 43, no. 10, pp. 2429–2443, 2015.
- [56] G. D. Caserta, L. Iannucci, and U. Galvanetto, "Shock absorption performance of a motorbike helmet with honeycomb reinforced liner," *Compos. Struct.*, vol. 93, no. 11, pp. 2748–2759, 2011.
- [57] P. Halldin, "Energy absorption Biomechanics and neuronics."
- [58] B. Croop, H. Lobo, and N. DatapointLabs, "Selecting material models for the simulation of foams in LS-DYNA," *Proc. 7 th LS-DYNA ...*, 2009.
- [59] R. M. Coelho, R. J. Alves de Sousa, F. A. O. Fernandes, and F. Teixeira-Dias, "New composite liners for energy absorption purposes," *Mater. Des.*, vol. 43, pp. 384–392, 2013.

